RESEARCH

2007-37

Automated Winter Road Maintenance Using Road Surface Condition Measurements

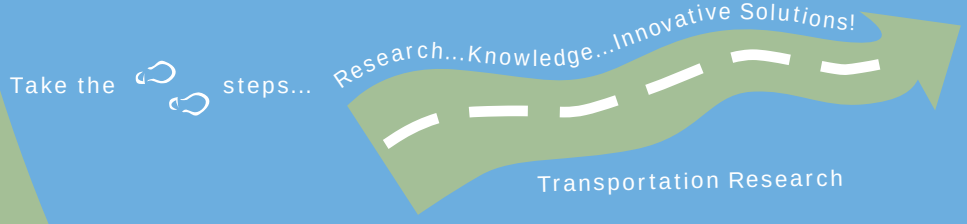

Technical Report Documentation Page

1. Report No.	2.	3. Recipients Accession No.
MN/RC 2007-37		

4. Title and Subtitle	5. Report Date
Automated Winter Road Maintenance Using Road Surface Condition Measurements	September 2007
	6.

7. Author(s)	8. Performing Organization Report No.
Gurkan Erdogan, Lee Alexander, Piyush Agrawal, and Rajesh Rajamani	

9. Performing Organization Name and Address	10. Project/Task/Work Unit No.
University of Minnesota Department of Mechanical Engineering 111 Church Street, S.E. Minneapolis, MN 55455	11. Contract (C) or Grant (G) No. (c) 81655 (wo) 148

12. Sponsoring Organization Name and Address	13. Type of Report and Period Covered
Minnesota Department of Transportation 395 John Ireland Boulevard Mail Stop 330 St. Paul, Minnesota 55155	Final Report 14. Sponsoring Agency Code

15. Supplementary Notes
http://www.lrrb.org/PDF/200737.pdf

16. Abstract (Limit: 200 words)

Real-time measurement of tire-road friction coefficient is extremely valuable for winter road maintenance operations and can be used to optimize the kind and quantity of the deicing and anti-icing chemicals applied to the roadway.

In this project, a wheel based tire-road friction coefficient measurement system is first developed for snowplows. Unlike a traditional Norse meter, this system is based on measurement of lateral tire forces, has minimal moving parts and does not use any actuators. Hence, it is reliable and inexpensive. A key challenge is quickly detecting changes in estimated tire-road friction coefficient while rejecting the high levels of noise in measured force signals. Novel filtering and signal processing algorithms are developed to address this challenge including a biased quadratic mean filter and an accelerometer based vibration removal filter.

Detailed experimental results are presented on the performance of the friction estimation system on different types of road surfaces. Experimental results show that the biased quadratic mean filter works very effectively to eliminate the influence of noise and quickly estimate changes in friction coefficient. Further, the use of accelerometers and an intelligent algorithm enables elimination of the influence of driver steering maneuvers, thus providing a robust friction measurement system.

In the second part of the project, the developed friction measurement system is used for automated control of the chemical applicator on the snowplow. An electronic interface is established with the Force America applicator to enable real-time control. A feedback control system that utilizes the developed friction measurement sensor and a pavement temperature sensor is developed and implemented on the snowplow.

17. Document Analysis/Descriptors	18. Availability Statement
Tire-road friction, friction measurement, winter road maintenance, automated winter maintenance, redundant tire based friction measurement, piezoelectric sensors	No restrictions. Document available from: National Technical Information Services, Springfield, Virginia 22161

19. Security Class (this report)	20. Security Class (this page)	21. No. of Pages	22. Price
Unclassified	Unclassified	89	

Automated Winter Road Maintenance Using Road Surface Condition Measurements

Final Report

Prepared by:

Gurkan Erdogan
Lee Alexander
Piyush Agrawal
Rajesh Rajamani

Department of Mechanical Engineering
University of Minnesota

September 2007

Published by:

Minnesota Department of Transportation
Office of Research Services
Mail Stop 330
395 John Ireland Boulevard
St. Paul, Minnesota 55155

Acknowledgements

This research was funded by the Minnesota Department of Transportation (MNDOT) under Contract No. 81655. We also thank MnDOT for access to the snowplow and for other resources provided during the project.

Table of Contents

List of Tables

List of Figures

Executive Summary

Real-time measurement of tire-road friction coefficient is extremely valuable for winter road maintenance operations. Knowledge of tire-road friction coefficient can be used to optimize the kind and quantity of the deicing and anti-icing chemicals applied to the roadway.

In this project, a wheel based tire-road friction coefficient measurement system is first developed for snowplows. Unlike a traditional Norse meter, this system is based on measurement of lateral tire forces, has minimal moving parts and does not use any actuators. Hence, it is reliable and inexpensive. A key challenge is quickly detecting changes in estimated tire-road friction coefficient while rejecting the high levels of noise in measured force signals. Novel filtering and signal processing algorithms are developed to address this challenge including a biased quadratic mean filter and an accelerometer based vibration removal filter.

Detailed experimental results are presented on the performance of the friction estimation system on different types of road surfaces. Experimental results show that the biased quadratic mean filter works very effectively to eliminate the influence of noise and quickly estimate changes in friction coefficient. Further, the use of accelerometers and an intelligent algorithm enables elimination of the influence of driver steering maneuvers, thus providing a robust friction measurement system.

In the second part of the project, the developed friction measurement system is used for automated control of the chemical applicator on the snowplow. An electronic interface is established with the Force America applicator to enable real-time control. A feedback control system that utilizes the developed friction measurement sensor and a pavement temperature sensor is developed and implemented on the snowplow. The working of the automated control system is documented through videos.

Finally, in an early unsuccessful portion of the project, the use of piezoelectric sensors for estimation of tire-road friction coefficient and slip angle was evaluated. The results from this portion of the project are also described in this report.

Experimental results obtained in the project show that reasonably accurate estimates of slip angle could be obtained using the new piezoelectric sensors, especially on high friction coefficient surfaces. However, reliable estimates of friction coefficient could not be obtained. Significant additional work is needed before the piezoelectric sensors could be used in a real-world application on the snow plow for estimating tire-road friction coefficient. It was therefore decided that the piezoelectric sensors will not be used further in this project for closed-loop control of pavement material application on the snowplow. Instead the wheel and load-cell based system was used for estimation of tire-road friction coefficient and closed-loop material application control.

Chapter 1

DEVELOPMENT OF WHEEL-BASED FRICTION MEASUREMENT SYSTEM

1.1 Introduction

Determining the optimum amount of chemicals that need to be applied for maintaining a safe road surface condition in winter is an application where measurement of tire-road friction coefficient could be utilized effectively. Many highway agencies in Europe, Japan, and the U.S. have come to believe that surface friction measurements may form the basis for improved winter maintenance operations and mobility [1]. Efficient use of deicing material, correct location and time for the maintenance, minimum environmental damage and cost are the main goals for the design of an advisory or automated system.

Several research papers ([5] – [9]) have been published so far about vehicle-based tire road friction coefficient estimation. These systems are based on measurement of the vehicle's motion through sensors such as GPS, lateral and longitudinal accelerometers, wheel speed and yaw rate. However, most of these proposed systems require a certain amount of slip of the vehicle's tire, either through acceleration-deceleration maneuvers or else through steering maneuvers. The friction coefficient cannot be estimated when neither acceleration, deceleration nor steering occurs [3].

Wheel based friction measurement systems utilize a redundant wheel and are appropriate for heavy duty trucks such as snowplows. The Norse meter is a commercialized wheel based system which is used in winter road maintenance. This system requires a dedicated operator and an actuator to skid the additional wheel on the roadway at timed intervals. The new wheel based system described in this report for the same purpose has several advantages over this traditional system.

The wheel based system developed in this project employs an additional wheel which is at an angle with the traveling direction of the snowplow. Due to the angle, namely the slip angle, a continuous lateral force is generated at the tire. The continuous force signal enables the design of an autonomous system which is very beneficial for the maintenance of roadways. The measured lateral force signal is filtered and processed in real time with the help of some novel algorithms developed for reliably estimating the tire-road friction coefficient. The road surface condition is precisely evaluated with the tire-road friction coefficient and a control signal is sent to the applicator using the output of a change detection algorithm.

1.2 Autonomous Winter Road Maintenance System

1.2.1 System Specifications

The designed Automated Winter Road Maintenance System is composed of an additional

wheel, a load cell, a data processing unit and the deicing applicator of the snowplow. The additional wheel is located near the front axle of the snowplow, while the deicing applicator is located at the back as in Figure 1.1.

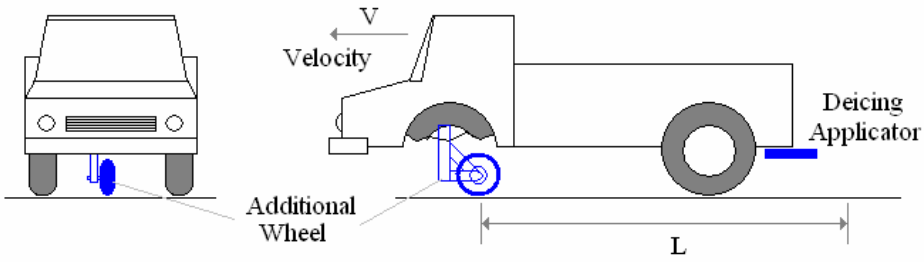

Figure 1.1 Winter Road Maintenance System

Since a real-time system is desired, only a limited time is available for data processing. The available data processing time depends up on the vehicle's speed and the distance from the wheel to the applicator. In other words, after the additional wheel passes over a surface transition, the processor has a total time of L/V seconds to send a control signal to the applicator. Minimum available time occurs at the highest snowplowing speed and the goal is to keep the data processing time less than the minimum available time. Various snowplowing speeds and corresponding available times are listed in table 1.

Truck Speed [mph]	Available Time [msec]
20	671
30	447
40	336
50	268

Table 1.1 Truck Speeds vs. Available Times for Data Processing

1.2.2 Friction Coefficient Measurement System

A top view schematic and a side view photo of the developed wheel based system are given in Figure 1.2. The additional wheel stands at an angle with its traveling direction. This angle is called the tire slip angle and it causes the tire to generate a lateral force continuously [3]. A pneumatic dashpot with a constant air pressure applies a constant normal force to the wheel. Since the normal tire force is fixed and since the slip angle is large ($\alpha \cong 5^o$) enough, the lateral force is proportional to the tire-road friction coefficient. By measuring the lateral tire force and after adequate signal processing, one can estimate the tire-road friction coefficient.

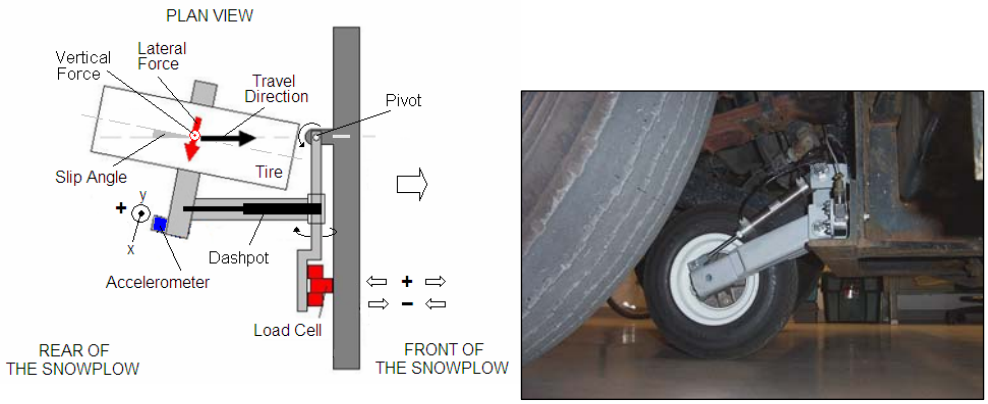

Figure 1.2 Wheel Based System

A pancake type load cell is used to measure the lateral force through the moment arm turning about the pivot as indicated in Figure 1.2. The load cell produces a negative voltage under compression forces and a positive voltage under tension forces. Only the lateral tire forces at the contact patch are measured by the load cell since the centerline of the contact patch is aligned with the vertical hinge. An inexpensive, two dimensional MEMS accelerometer is used to detect and filter out the noise on the force signal. X axis measures the lateral acceleration while Y axis measures the vertical acceleration of the center of the additional wheel. The vertical axis of the accelerometer produces a positive voltage while accelerating in the upward direction and a negative voltage while accelerating in the downward direction.

1.3 Fundamental Technical Challenges

1.3.1 Technical Challenges

There are two main technical challenges to be addressed in developing a friction estimation algorithm with the proposed redundant wheel based system.

1) Enormous Noise on the Force Signal

A major technical challenge in the design of the wheel based system is the excessive noise on the load cell signal mainly caused by the oscillations of the truck body or the excitations from the bumps and dips on the roadway. Due to the high variance of the noise on the force signal, it is hard to detect any change on the road surface by using the raw force signal, as seen in Figure 1.3.

2) Variations due to Steering

When the driver is steering, the lateral forces measured by the instrumented wheel changes. It is important to compensate for these changes in order to correctly identify the tire-road friction coefficient.

1.3.2 Physical Interpretation of Noise Generating Mechanism

A typical force signal measured by the load cell and an arithmetic mean (AM) filtered version of it are given in Figure 1.3. The force is measured while the snowplow is traveling

on a dry asphalt road in the first four seconds and on an icy road in the following four seconds. The step change due to the road surface transition at the fourth second cannot be easily distinguished because of the high variance of the noise, especially on the dry asphalt region. A careful analysis of the system and the force signal reveal some clues about the dominant noise generating mechanism and the associated frequency bands.

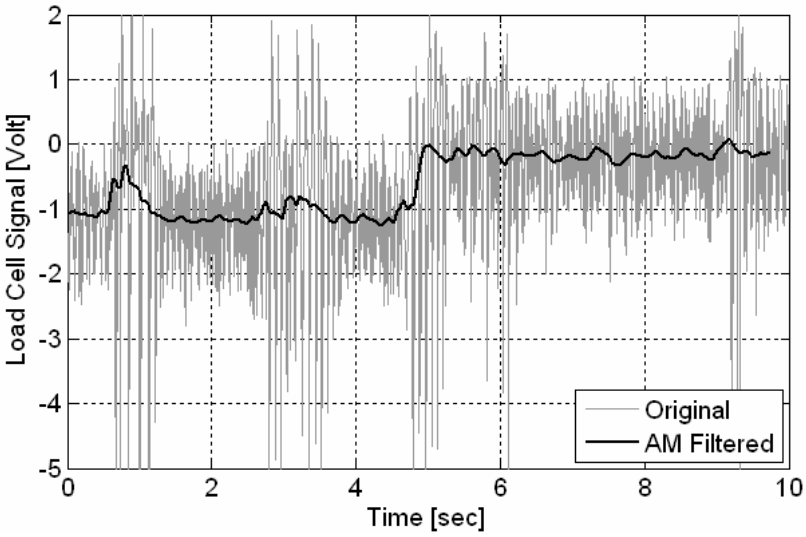

Figure 1.3 Typical Force Signal

When we take a closer look at the noise on the dry asphalt region, we see that the signal is negatively skewed, meaning that the tail of the distribution under the mean is longer than the tail of the distribution over the mean. We can also see that the absolute mean value of the signal decreases as the variance of the signal increases. The physical interpretation of this type of behavior is explained in the following paragraphs and the disturbances coming from the roadway play an important role as a noise generating mechanism in this interpretation.

As we have mentioned previously, the wheel based system is designed in such a way that the load cell only measures the lateral tire force (F_{Lat}) which is a function of both the tire-road friction coefficient (μ) and the normal tire force (F_N) as presented in equation 1.1.

$$F_{Lat} = \mu \times F_N \tag{1.1}$$

The pneumatic dashpot applies a constant normal force to the additional wheel, but does not really help to reduce the tire deflections due to the disturbances coming from the roadway. So, the roughness of the roadway introduces a high frequency noise on the normal tire force which engenders a similar type of noise on the lateral tire force according to the equation 1.

Each time the additional wheel passes over a relatively bumpy spot on the roadway, it vertically starts to vibrate between the ground and the dashpot. The negative skewness of the lateral tire force is due to the transient normal forces occurring as the wheel bounces from the ground, while the reduction of the absolute mean value of the signal is due to the low impedance of node on the dashpot side. In other words, the vertical vibrations of the wheel loosen the contact patch between the tire and the road, causing a reduction in the lateral

force. This slower change in the lateral tire force can be seen on an arithmetic mean filtered force signal as in Figure 1.3. In summary, as an inherent property of the designed system, the absolute mean value of the force signal decreases whenever the variance of the force signal increases.

This interpretation can best be proved by the high correlation coefficient observed between the vertical acceleration and the load cell signals at high frequencies. This will be discussed in more detail in the following sections.

1.3.3 Frequency Content of Force Signal

The FFT spectrum of a typical force signal measured on a dry asphalt road is given in figure 4. By using this frequency spectrum we can clarify what a meaningful signal is and define which frequency ranges correspond to low and high frequency noise.

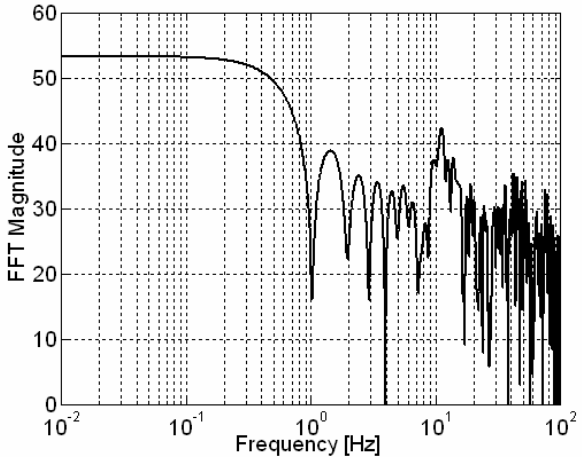

Figure 1.4 FFT Spectrum of a Typical Force Signal

A meaningful signal is a change in the force signal only due to a road surface change. We assume that the frequency content of the noiseless signal is very close to zero frequency, i.e. to the DC component. The low frequency noise corresponds to the frequencies lower than 1 Hz excluding the DC component, whereas the high frequency noise corresponds to the frequencies higher than 1 Hz. The energy of the high frequency noise of a typical force signal is mainly centered between 10 Hz and 20 Hz as seen in Figure 1.4.

1.4 Filter Development

1.4.1 Low Pass Filter Performance

Our goal is to design a digital filter that can filter out all the excessive noise while preserving the step changes due to the road surface change. According to figure 4, this implies a filter with a cut off frequency close enough to zero frequency (~0.1Hz) and as a specification, a sufficient amount of noise reduction (~25dB) at low frequencies (~0.5Hz).

It is not possible to design a linear low pass filter that could meet both the filtering specifications and the data processing time constraint due to the real-time requirements of the system. As an example, a 2^{nd} order Butterworth low pass filter is designed in MATLAB for

removing the noise. The frequency response of the designed filter is given in Figure 1.5. The cut-off frequency is picked at 1 Hz so that its time constant is approximately 200 milliseconds. However, the performance of this filter in terms of reducing the influence of vibrations is not satisfactory, as presented in Figure 1.5. Consequently, new filtering algorithms need to be developed for removing very low frequencies in a reasonable time.

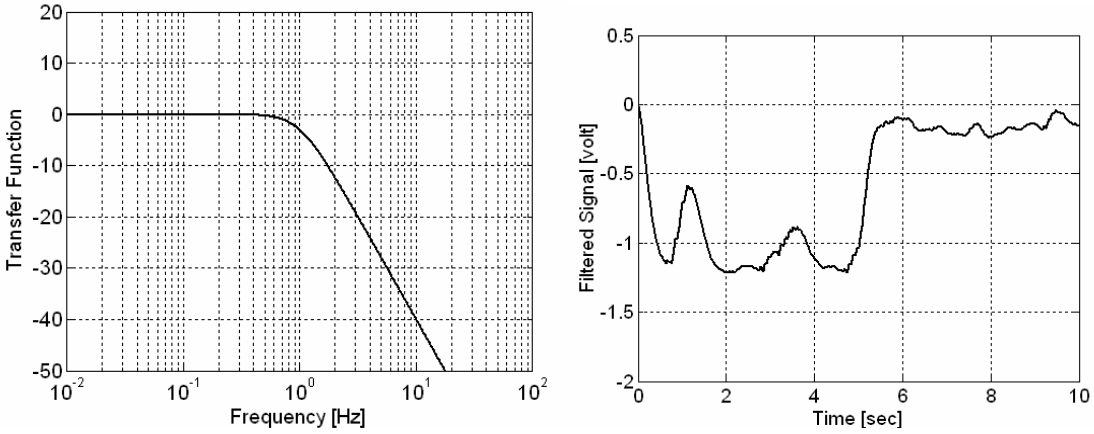

Figure 1.5 2nd Order Butterworth Low Pass Filter and the Filtered Signal

1.4.2 Design Based on Biased Quadratic Mean Filter

A new filter is designed based on a modified quadratic mean filter (QMF) by exploiting the relationship between the mean and the variance of the force signal which is inherent in the dynamics of the proposed friction coefficient measurement system as discussed previously. The variance takes care of filtering the low frequency oscillations on the force signal, leading to a faster and better filtering performance at low frequency bands.

The definition of a QMF is given in equation 1.2, where x_i is the sampled signal, m is the number of samples in a moving time window and N is the size of the sampled signal.

$$y_j = \sqrt{\frac{1}{m}\sum_{i=j}^{j+(m-1)}(x_i)^2} \qquad j = 1 : N-(m-1) \tag{1.2}$$

The output of QMF is nothing but the (moving) root mean square (RMS_j) of the signal which can be written in terms of the moving average (μ_j) and variance (σ_j^2) of the signal as in equation 1.3 [4].

$$y_j = RMS_j = \sqrt{\mu_j^2 + \sigma_j^2} \tag{1.3}$$

The quadratic mean filter can be modified to utilize the dynamic relationship between the mean and the variance for removing the low frequency oscillations. The new biased quadratic mean filter algorithm introduces a constant bias (K) which is unique to the measurement system and valid for all snowplow speeds.

$$y_j = -\sqrt{\frac{1}{m}\sum_{i=j}^{j+(m-1)}\left(x_i + K\right)^2} - K \qquad j = 1 : N-(m-1) \tag{1.4}$$

From equation 1.4, the following relation between the moving average $\left(\mu_j\right)$ and the variance $\left(\sigma_j^2\right)$ can be deduced:

$$y_j = -\sqrt{\sigma_j^2 + \left(\mu_j + K\right)^2} - K \qquad j = 1 : N-(m-1) \tag{1.5}$$

The proof of this relation is given in equation 1.6.

$$\begin{aligned} y_j &= \sqrt{\frac{1}{m}\sum_{i=j}^{j+(m-1)}\left(x_i + K\right)^2} \\ &= \sqrt{\frac{1}{m}\sum_{i=j}^{j+(m-1)} x_i^2 + \frac{1}{m}\sum_{i=j}^{j+(m-1)} 2x_i K + \frac{1}{m}\sum_{i=j}^{j+(m-1)} K^2} \\ &= \sqrt{\frac{1}{m}\sum_{i=j}^{j+(m-1)}\left(x_i - \mu_j + \mu_j\right)^2 + 2K\ \mu_j + K^2} \\ &= \sqrt{\frac{1}{m}\sum_{i=j}^{j+(m-1)}\left(x_i - \mu_j\right)^2 + 2\mu_j^2 - \mu_j^2 + 2K\ \mu_j + K^2} \\ &= \sqrt{\sigma_j^2 + \left(\mu_j + K\right)^2} \end{aligned} \tag{1.6}$$

As we have explained previously, the absolute mean value of the force signal decreases/increases whenever the variance of the force signal increases/decreases according to the physical interpretation of the system. This implies that the low frequency oscillation on the square mean value $\left(\mu_j^2\right)$ signal is approximately 180^o out of phase with the low frequency oscillation on the variance $\left(\sigma_j^2\right)$. Hence, an appropriate bias value should be chosen so that the oscillations on both signals cancel out each other. If the magnitude of the square mean value oscillations is less than the magnitude of variance oscillations, K should have the same sign as μ_j.

If we assume that the oscillations on the $\left(\mu_j + K\right)^2$ signal and the variance have the same magnitude and are perfectly out of phase, by adding them up we can completely remove the low frequency oscillations and find a constant output such as $y_j = A$ which only changes with respect to the friction coefficient as is shown in Figure 1.6.

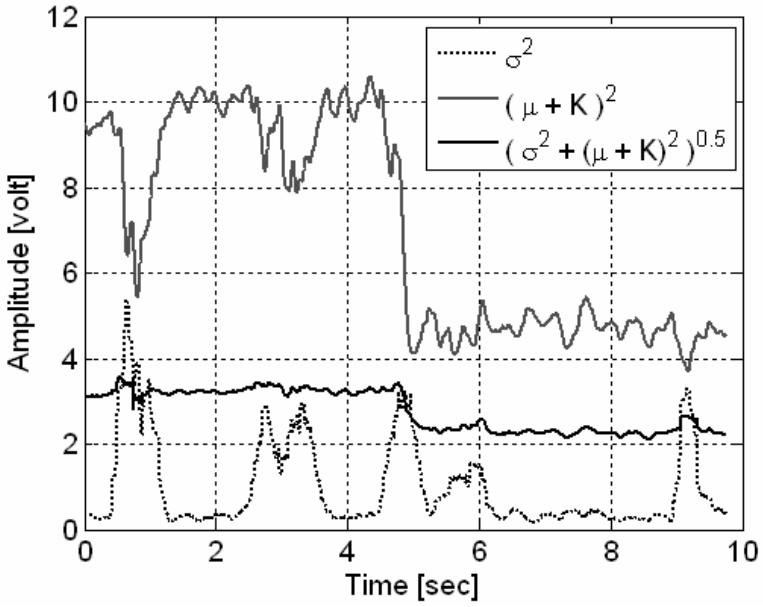

Figure 1.6 Biased Quadratic Mean Filter

We can write the mean value as a function of the standard deviation.

$$\mu_j = \sqrt{(A+K)^2 - \sigma_j^2} - K \tag{1.7}$$

We could solve equation 1.7 for the bias value, if we know the noise statistics and the exact value of the current friction coefficient. Alternately, we can also use the statistics and the mean value over a long period of time to update the value of the bias.

A Hann type weighting function is used while averaging the time windows. The Hann window is mostly effective in the filtering of high frequency bands rather than the low frequency bands.

1.4.3 New Filter Design Aided by Accelerometer Measurements

An alternate new filter, aided by accelerometer measurements, is designed to remove both low and high frequency noise from the signal. An accelerometer, measuring the vertical accelerations, is located at the center of the additional wheel as in Figure 1.7.

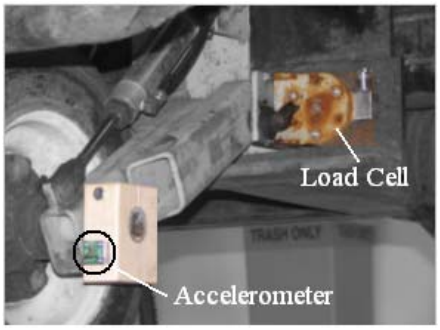

Figure 1.7 Accelerometer and Load Cell Locations

Smoothed force and acceleration signals are plotted together for a 400msec time span in Figure 1.8. This plot clearly shows that the high frequency noise (~10Hz) on the force and the vertical acceleration signals are inversely correlated. This also supports the assumption that the high frequency content of the measured lateral force signal is mostly due to the high frequency changes in the normal tire force caused by the roughness of the roadway. The acceleration signal can be utilized to remove the noise since it is related to the variance of the noise while being indifferent to the step changes of the force signal

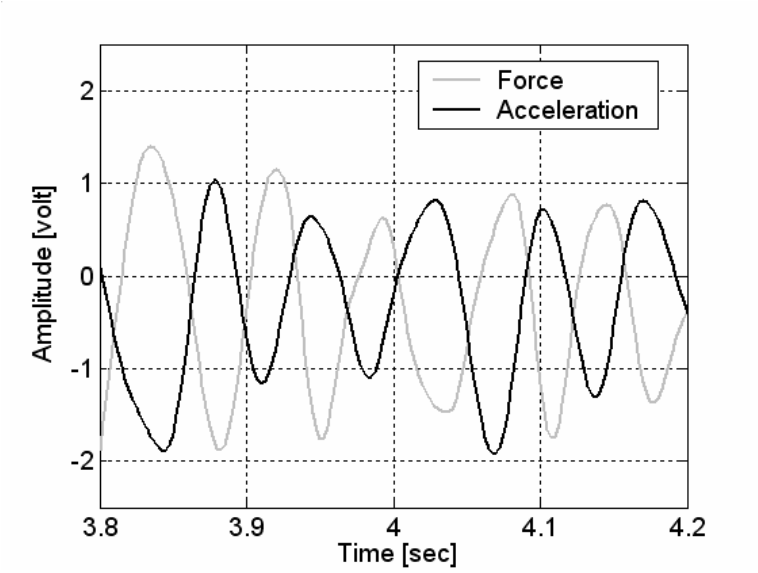

Figure 1.8 Force and Acceleration Signals

When we look at the force and the acceleration signals together, we see a certain amount of time delay between them. Because of this time delay and the excessive noise, the raw signals do not seem to be correlated enough to be utilized directly in a filter design. However, the correlation coefficient between these two signals can be increased significantly by simply smoothing the signals and shifting them with respect to each other.

After smoothing out both signals with an arithmetic mean filter using a Hann window, the shifting process is applied. The shifting algorithm is defined as follows;

- Predefine a set of time (time-step in discrete time) delays as in equation 1.8.

$$P = \{-3,-2,-1,0,1,2,3\} \tag{1.8}$$

- Shift the accelerometer signal as much as the time delay values in the set, once at a time.

- Calculate the correlation coefficient between the force and the shifted accelerometer signal for each and every time delay in the set P.

$$C_{yf}(p) = \frac{\sigma_{yf}(p)}{\sqrt{\sigma_{yy}\,\sigma_{ff}}} \tag{1.9}$$

- Find the required shift corresponding to the time delay that maximizes the correlation coefficient

$$\bar{p} = \{p : p \in P \quad \& \quad C_{yf}(p) = \max[C_{yf}(p)]\} \tag{1.10}$$

The time delay set can be expanded according to the anticipated time delay range and the capacity of the processor. There is no unique time delay between the signals, so we have to update the time delay between the signals in every time step. However, this updating process can be done less frequently, if the desired data process time is exceeded.

Finally, the algorithm requires the addition of smoothed and shifted versions of accelerometer and load cell signals in every time step to cancel out noise on the force signal. The sum is passed through a secondary arithmetic mean filter to remove the higher frequency components of the noise.

1.4.4 Comparing Filter Performances

A performance metric can be defined for assessing the filter performances in terms of the main goal of the system. Signal-to-noise ratio, as it is given in equation 1.11, is one way of defining such a metric. In this formula, “high” and “low” subscripts indicate two different levels of the signal, namely the dry asphalt and icy road regions respectively. The signal-to-noise ratio basically gives an idea how reliably a filtered signal could be used in a change detection algorithm

$$SN = \frac{\sigma_{high} + \sigma_{low}}{\mu_{high} - \mu_{low}} \times 100 \tag{1.11}$$

The signal-to-noise ratio comparison of the filters is presented in table 2. The cut-off frequency of the Butterworth filter in this table has been increased to 1Hz, so that it is fast enough to be within the limits of the real-time system and comparable with the designed filters.

Low Pass Filters	Signal to Noise Ratio
Butter Worth Filter	1.9
Quadratic Mean Filter	4.0
Accelerometer Aided Filter	7.8

Table 1.2 Performances of Different Filters

Results show that both of the designed filters perform better than a typical linear low pass filter. Further, the vertical acceleration signal seems to contribute to the filtering performance significantly. The experimental results provided at various snowplow speeds are pretty much compatible with this ranking.

Another way of comparing filters is to look at their responses to a step change. A perfect step input is artificially added to a force signal measured on a dry asphalt road and the filter time delays are compared as in Figure 1.9. Here, again the cut-off frequency of the Butterworth filter is 1Hz, meaning that the filter already has a poor performance while filtering out low frequency noises. Again, both of the designed filters' time delays are shorter than the linear filter. The quadratic mean filter and the accelerometer aided filter have an approximate time delay of 250msec. Consequently, a snowplow traveling at speeds up to 50 mph can be reliably handled with the proposed accelerometer aided filter or biased QMF algorithms.

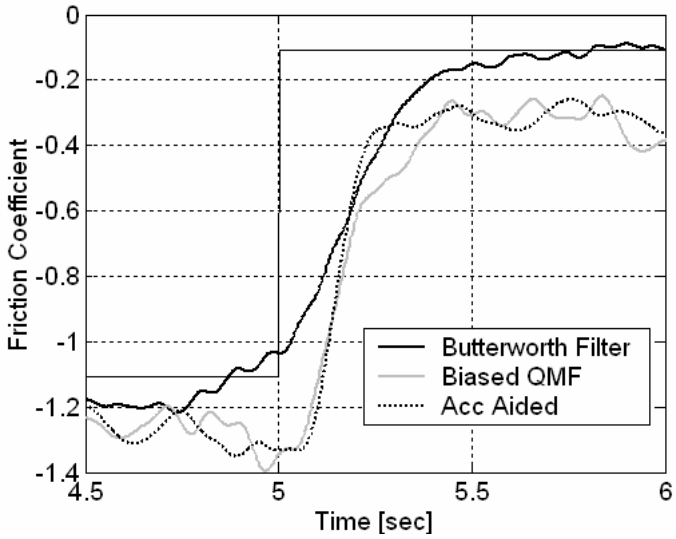

Figure 1.9 Time Delays of Different Filters

1.4.5 Change Detection Algorithm

The probability density function is a function of the random variable (y), i.e. the observed data, and the distribution parameter vector (□). In our case, observed data is the filtered data. Likelihood is defined as the probability of observing the same set of data. The likelihood function can be calculated as the product of the probability density of each sample. If we assume a Gaussian distribution, the likelihood function can be calculated as in equation 1.12.

$$p(y|\theta) = l(\theta|y) = \prod_{i=1}^{N} \frac{1}{\sqrt{2\pi\sigma^2}} e^{-\frac{1}{2}\left(\frac{y_i-\mu}{\sigma}\right)^2} \tag{1.12}$$

So, the question is that at what value of the distribution parameters the likelihood function becomes maxima. The answer to that question is easy for a Gaussian distribution, since the maximum likelihood estimator (MLE) for Gaussian distribution turns out to be the mean and the variance of the data.

A Gaussian distribution is assumed and the likelihood-ratio test statistic is the ratio between the likelihood evaluated at the MLE and the MLE subject to a restrictive parameter vector as in equation 1.13. This parameter vector is expected to converge to a certain value as more and more experiments are done.

$$\Lambda = 2\ln\left\{\frac{l(\theta|y)}{l(\theta_r|y)}\right\} = -2\ln\left\{\frac{l(\theta_r|y)}{l(\theta|y)}\right\} = -2\left\{L(\theta_r|y) - L(\theta|y)\right\} \tag{1.13}$$

Then, a hypothesis test can be employed and applied to the likelihood ratio with a predefined threshold. If the threshold is exceeded, a control signal is sent to the applicator as in Figure 1.10. Again, the value of the threshold will be assigned more realistically as the number of road tests increases.

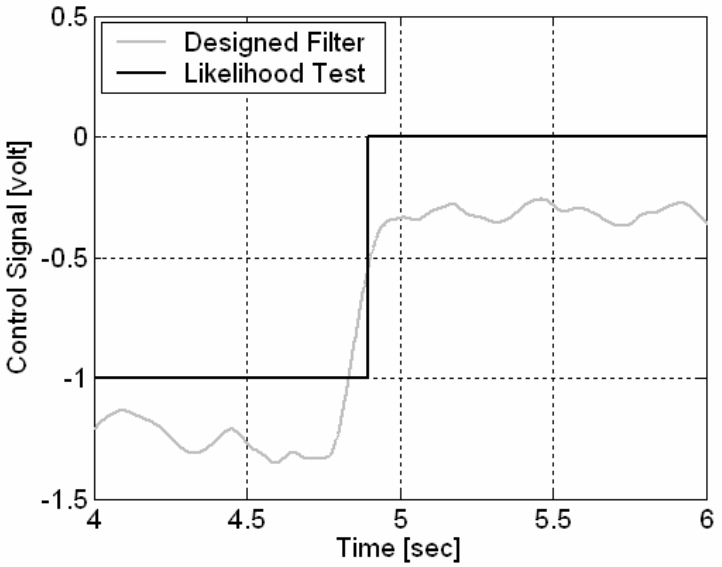

Figure 1.10 Hypothesis Test by Using Likelihood Ratio Test

Chapter 2
EVALUATION OF WHEEL-BASED FRICTION MEASUREMENT SYSTEM

2.1 Snowplow and Experimental Hardware

The vehicle used to conduct the experiments is a full sized snowplow (referred to as SAFEPLOW) manufactured by Navistar International Truck Company as shown in Figure 2.1.

Figure 2.1 The SAFEPLOW used for the experiments

The front axle of the snowplow had Goodyear G159 11R24.5 tires while the rear axle had dual Goodyear G124 11R 24.5tires. A computer data acquisition, signal processing and real-time control system were utilized. The real-time software consisted of C-code written for quasi real-time operation in the Windows operating system. The sampling frequency utilized was 400 Hz. A PCI Sensorray 626 data acquisition system which provided 16 channels of 16-bit analog-to-digital conversion and 4 channels of analog outputs was utilized. A Sensotec load cell for force measurements and dual axis accelerometers from Analog Devices were the primary sensors that were used.

2.2 Eliminating the Effect of Steering

The steering of the snowplow also contributes to unwanted changes in lateral force. This happens because steering introduces a new slip angle at the tire, thus changing the lateral

forces produced by the tire. The effect of steering can be eliminated either by modifying the system mechanically or by compensating for the steering in the algorithm with the help of a steering angle sensor or lateral accelerometer. In the current version of the system a lateral accelerometer, as in Figure 2.2, is used to compensate for the steering effect.

Original force and accelerometer signals and their low pass filtered (LPF) versions are presented in Figure 2.2a. The filtered accelerometer signal should be shifted and scaled with respect to the force signal, in order to compensate for the steering variations in the force.

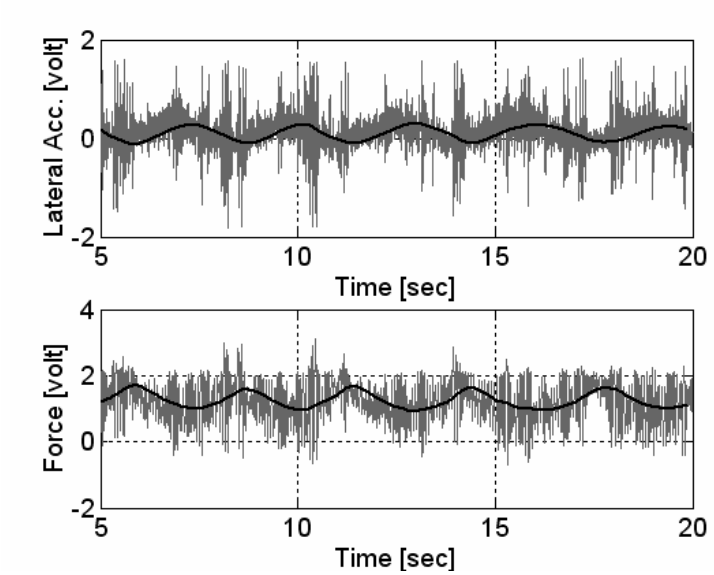

(a)

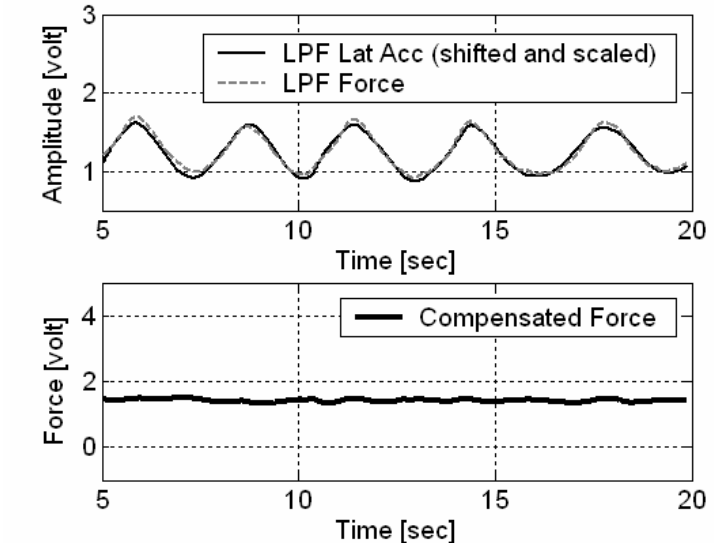

(b)

Figure 2.2 Steering Effect of the Snowplow

The cross-correlation based approach, as in section 1.3 for the accelerometer aided filter algorithm, is used to find the necessary time delay. The scaling factor can be set to an initial value and updated over a long period of time. The scaled and shifted version of LPF lateral

acceleration signal is plotted together with the LPF force signal in Figure 2.2b. Taking the difference between two signals compensates the steering effect of the force signal remarkably, as presented in figure11b.

2.3 Detailed Experimental Results

Several tests are done to evaluate the performance of the designed autonomous road maintenance system. First, the effects of acceleration, deceleration and steering maneuvers on the measurement system are examined. And then, the developed filtering algorithms are tested in the skid-pad having a surface transition from dry asphalt to ice, at different snowplow speeds.

2.3.1 Effects of Acceleration, Deceleration and Steering

The vertical and the longitudinal forces at the contact patch are not measured by the load cell since the centerline of the contact patch is aligned with the vertical hinge. This also means that the longitudinal acceleration and deceleration of the snowplow should not have any effect on the load cell measurements.

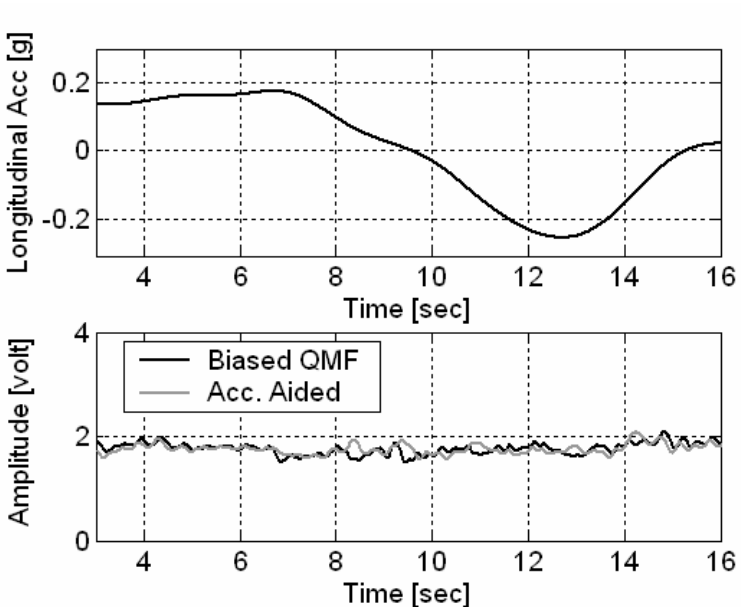

Figure 2.3 Effect of Acceleration and Deceleration of the Snowplow

A stationary snowplow is accelerated from zero to a maximum velocity (30mph), and then decelerated back to zero velocity and brought to a complete stop. The longitudinal acceleration of the redundant wheel is measured as in Figure 2.3 with the help of another accelerometer. The measured force signal is not significantly affected by the acceleration changes, as shown in Figure 2.3.

The effect of steering maneuvers has been discussed in section 2.2.

2.3.2 Skid-Pad Tests

Figure 2.4 Skid-Pad Test Environment

The test environment is a special, closed-to-traffic roadway with a length of approximately 0.5 km. The two thirds of the road surface is dry asphalt, while the rest is covered with hard ice. The transition from dry asphalt to icy road does not occur abruptly, rather gradually through a road surface composed of a mixture of wet asphalt and soft ice as in Figure 2.4.

The original force signal and the performances of the developed filters at different snowplow speeds are presented in Figure 2.5. The speeds, ranging from 10mph to 40mph, cover the speed range in which the snowplows operate in real-life during application control. The variance of the excessive noise on the original force signal tends to increase as the speed of the snowplow increases. Both filter algorithms perform well and operate fast enough to satisfy the real-time requirements of the system at different speeds.

However, in some of the measurements, it is observed that after a few seconds when the snowplow passes over the asphalt-to-ice transition, the output of the accelerometer aided filter falls remarkably. This type of behavior can be seen in the 30mph and 40mph truck speed plots, in Figure 2.5. A bumpy spot is determined on the icy roadway where this incident happens according to the time axis.

The reason for the poor performance of the accelerometer aided filter in this bumpy spot on the icy road is the reduction of the tire-road friction coefficient. The accelerometer measurements are highly affected by the vertical force oscillations coming from the roadway, but only a small portion of these vertical tire force oscillations are converted into the lateral tire force oscillations through equation 1.1 since the friction coefficient of the icy road is low. Because of the disproportional amplitude of vertical acceleration and lateral force signals, the accelerometer aided algorithm does not perform well enough while removing the excessive noise.

On the other hand, the biased quadratic mean filter performs better than the accelerometer aided filter, when the wheel passes over such a bumpy spot on the icy roadway. The reason for this is that the biased QMF uses the variance of the original force signal rather than the accelerometer signal to quantify the noise. In other words, the algorithm does not rely on equation 1.1 and so is not affected by any reduction of the friction coefficient.

In general, the accelerometer aided filter performs better on dry asphalt road with high noise levels, while biased QMF performs reasonably well on both dry and icy roads. Since QMF based filtering depends directly on the variations of the noise on the force signal, it is more reliable than the accelerometer aided filter, and thus recommended for snowplow application.

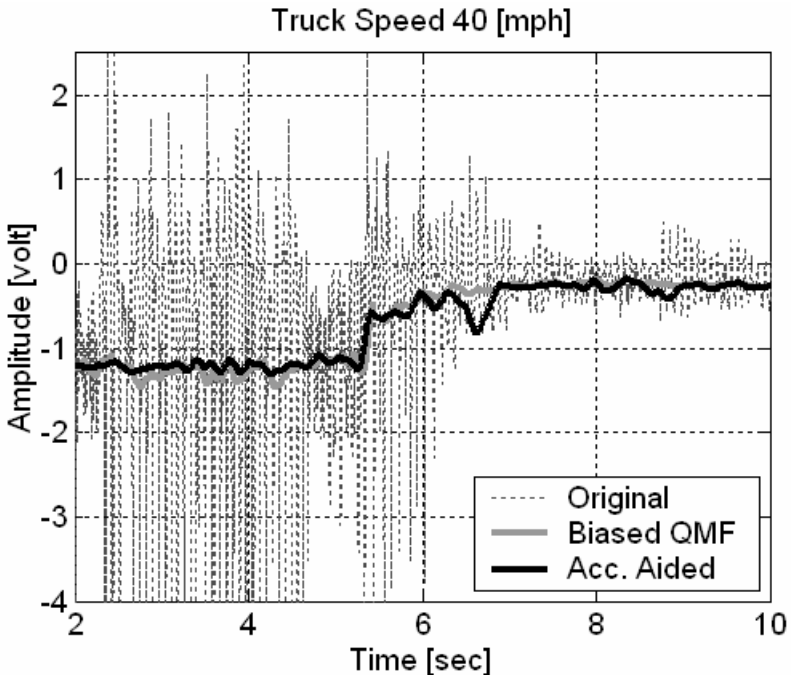
Truck Speed 40 [mph]
Amplitude [volt]
Time [sec]
Original
Biased QMF
Acc. Aided

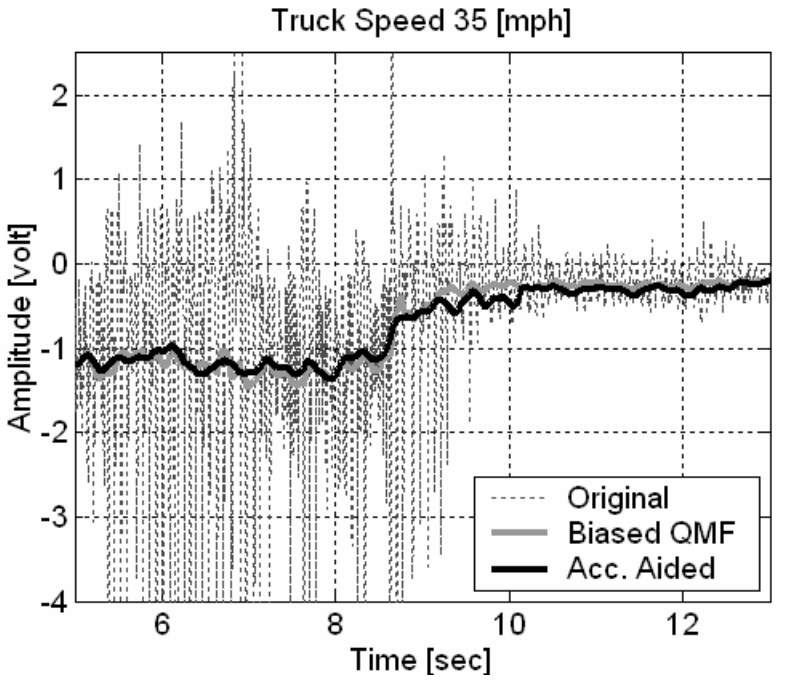
Truck Speed 35 [mph]
Amplitude [volt]
Time [sec]
Original
Biased QMF
Acc. Aided

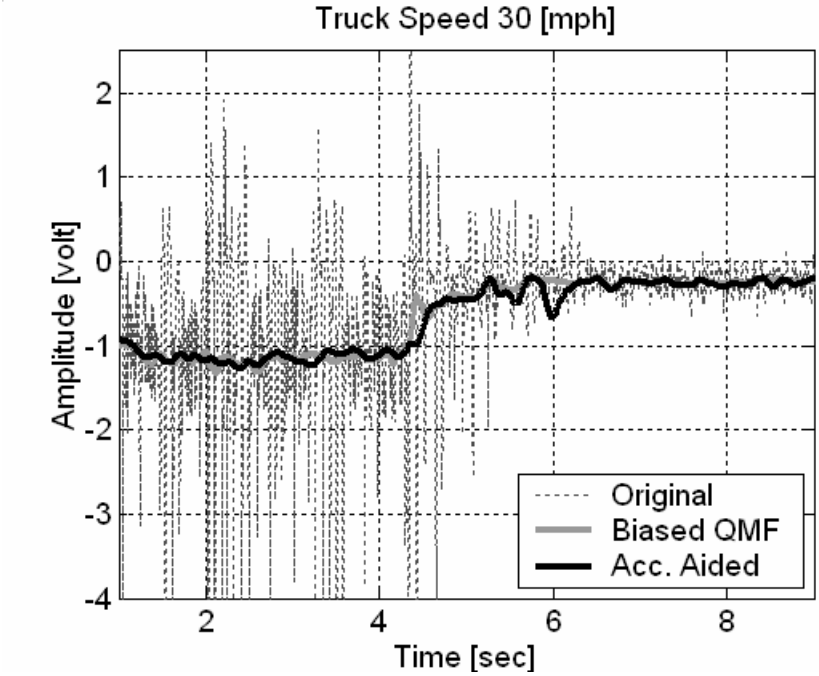
Truck Speed 30 [mph]
Amplitude [volt]
Time [sec]
Original
Biased QMF
Acc. Aided

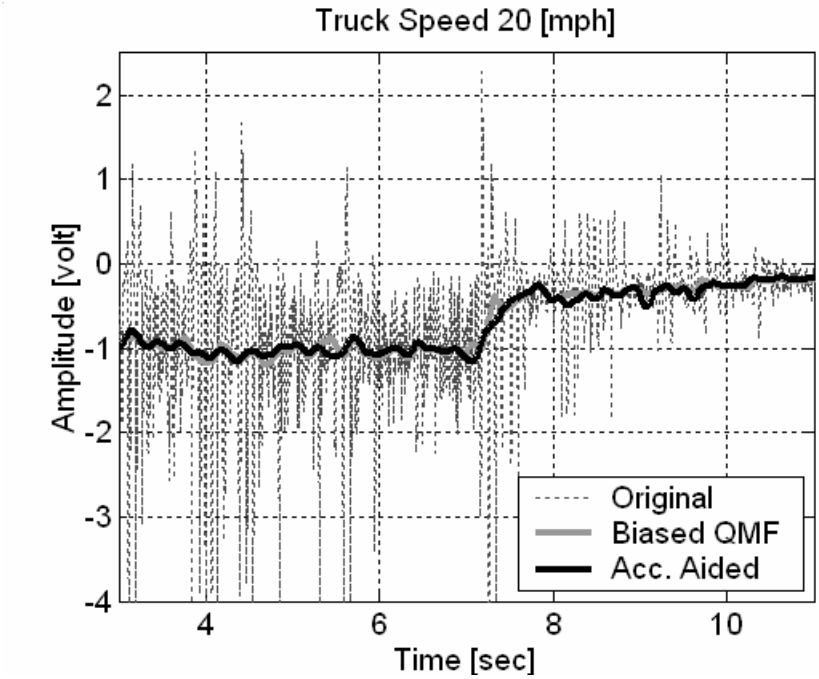
Truck Speed 20 [mph]
Amplitude [volt]
Time [sec]
Original
Biased QMF
Acc. Aided

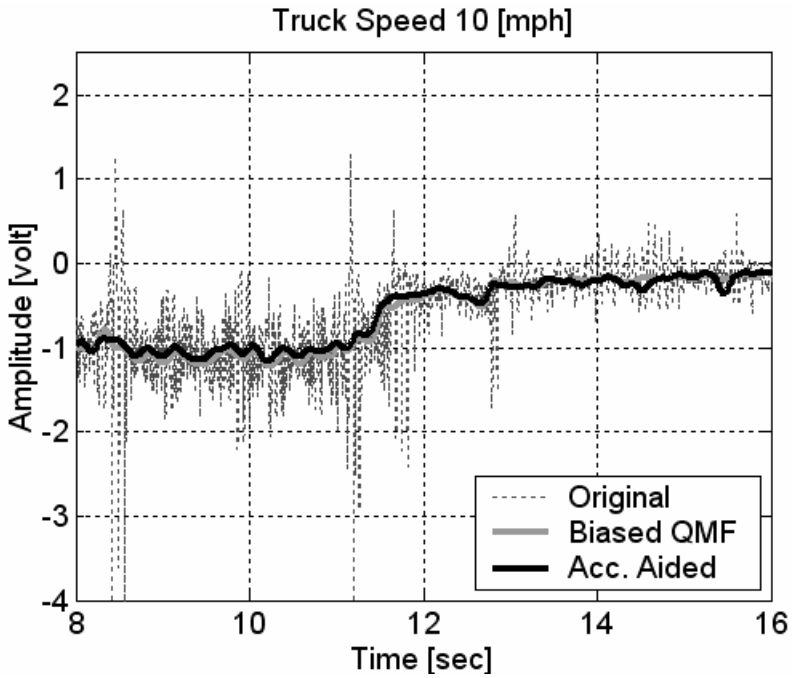

Figure 2.5 Test Results at Various Truck Speeds

2.4 Conclusions

This project developed a real-time autonomous winter road maintenance system employing friction coefficient estimation based on the tire force measurements of an additional wheel. However, the designed wheel based system is susceptible to excessive noise due to the roughness of the road surface and the key challenge is quickly detecting changes in tire-road friction coefficient while rejecting the high variance noise in measured force signals. New real-time filtering algorithms are developed to remove the noise especially in very low frequencies (<1Hz). Experimental results on the evaluation of a biased QMF and an accelerometer aided filter algorithm show that the biased QMF algorithm can work very efficiently to remove noise and quickly estimate changes in friction coefficient. The improvements in the filter performance have made it possible to run change detection algorithms such as the Likelihood-Ratio Test reliably.

Chapter 3
FEEDBACK CONTROL SYSTEM FOR AUTOMATIC APPLICATOR CONTROL

3.1 Computer Control Interface

An interface has been developed between the computer that calculates the current friction coefficient and the Force America (tm) deicing system hydraulics on the snowplow. The interface is as follows. The computer has a PCI based I/O board with a number of analog and digital I/O pins. The load cell that measures the lateral force being generated by the friction wheel is connected to one of the analog ports. When the friction-sensing program calculates that conditions are such that the deicing system should be activated it changes the state of one of the digital I/O pins. That pin is connected to a Kyotto KF0604D solid state relay that is in turn connected in parallel with the "Burst" switch on the Force America system. To turn the deicing applicator on the I/O port is actually turned "off" allowing it in to sink the 5-volt dc current supplied to the relay's other input thus turning the relay on. If the Force America system has been properly initialized to be ready to spread deicing chemicals using their menu system then either the manual "Burst" switch or the friction sensing computer can turn the applicator on.

We also connect to an RS 232 serial port on the RoadWatch (tm) pavement temperature sensor. This serial port transmits a hexadecimally encoded character string that contains the air temperature and the pavement temperature from a sensor mounted on the driver's side rear view mirror. After decoding this string the temperatures can be used along with the friction coefficient to determine whether or not to trigger the application of deicing chemical.

3.2 Closed-Loop Control System

The development of a closed-loop control system for automatic control of the deicing applicator has been done using the deicing application guidelines provided in the Minnesota Snowplow Operators Field Handbook. The specific table used has been included as an Appendix on page 28 of this report.

A graphical summary of the application guidelines for spot treatment is shown in Figure 3.1. Spot treatment with sand or other non-abrasive chemical for deicing is used when the pavement temperature is below $15^{o}F$. At temperatures between $15^{o}F$ and $25^{o}F$, uniform treatment with sand (or other alternate chemical) is used in the case of freezing rain. Spot treatment is not used in this case.

Hence the use of tire-road friction coefficient measurement and pavement temperature measurement for applicator control is useful in the case where pavement temperature is less than $15^{o}F$, since spot treatment is only used in this case. The control system therefore consists of real-time estimation of friction coefficient, real-time measurement of pavement

temperature and application of sand (or alternate non-abrasive chemical) in areas where the friction coefficient is less than 0.6. Note that the threshold 0.6 has been chosen arbitrarily by the researchers and can be set to any other value by MnDOT. Figure 3.2 provides a graphical summary of the control system. A preliminary evaluation of this control system has been conducted at the skid pad at St. Cloud State University and Highway Safety research Center. Videos documenting the performance of the control system are attached in the following CD.

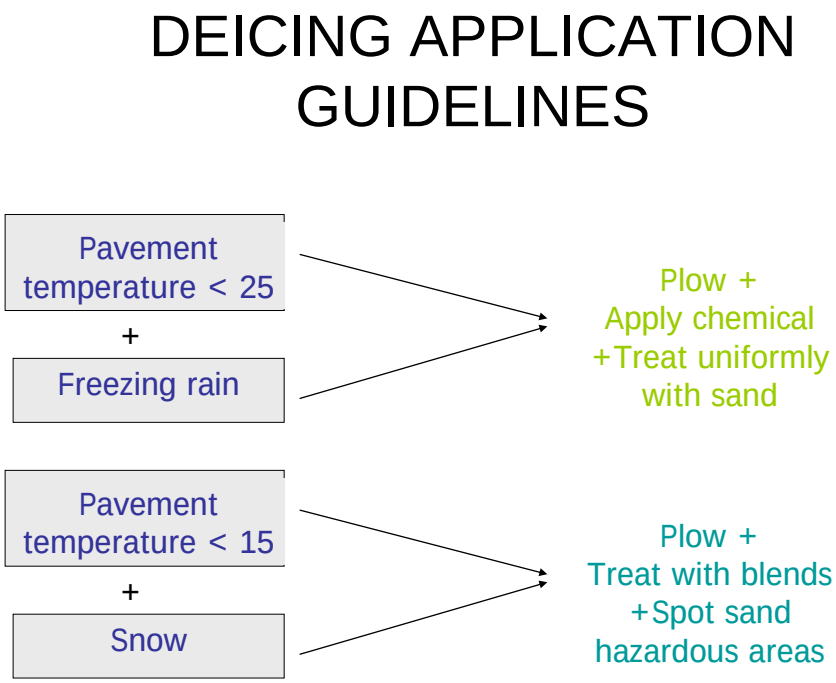

Figure 3.1 Guidelines for Deicing Application

CONTROL SYSTEM

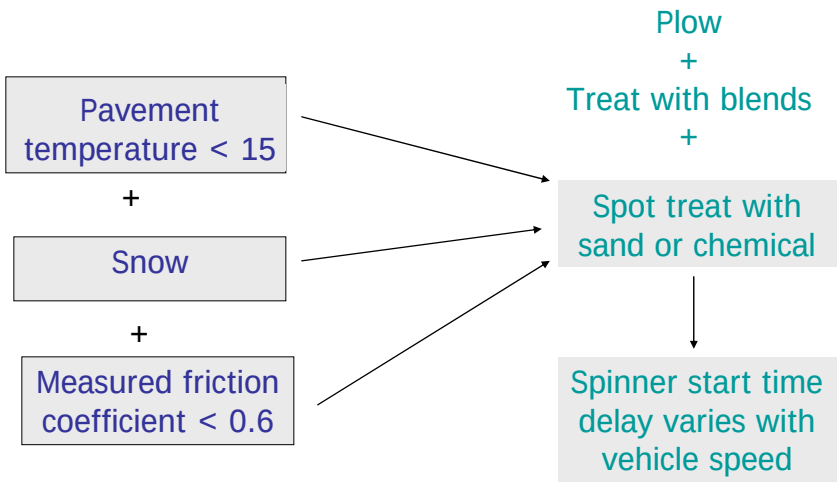

Figure 3.2 Control System for Automatic Applicator Control

Deicing Application Rate Guidelines
24' of pavement (typical two-lane road)

These rates are not fixed values, but rather the middle of a range to be selected and adjusted by an agency according to its local conditions and experience.

			Lbs/ two-lane mile			
Pavement Temp. (~F) and Trend ( )	Weather Condition	Maintenance Actions	Salt Prewetted/ Pretreated With Salt Brine	Salt Prewetted/ Pretreated With Other Blends	Dry Salt*	Winter Sand (abrasives)
>30°	Snow	Plow, treat intersections only	80	70	100*	Not recommended
	Frz. rain	Apply chemical	80 – 160	70 – 140	100 – 200*	Not recommended
30°	Snow	Plow & apply chemical	80 – 160	70 – 140	100 – 200*	Not recommended
	Frz. rain	Apply chemical	150 – 200	130 – 180	180 – 240*	Not recommended
25 - 30~	Snow	Plow & apply chemical	120 – 160	100 – 140	150 – 200*	Not recommended
	Frz. rain	Apply chemical	150 – 200	130 – 180	180 – 240*	Not recommended
25 - 30~	Snow	Plow & apply chemical	120 – 160	100 – 140	150 – 200*	Not recommended
	Frz. rain	Apply chemical	160 – 240	140 – 210	200 – 300*	400
20 - 25~	Snow or frz. rain	Plow & apply chemical	160 – 240	140 – 210	200 – 300*	400
20 - 25~	Snow	Plow & apply chemical	200 – 280	175 – 250	250 – 350*	Not recommended
	Frz. rain	Apply chemical	240 – 320	210 – 280	300 – 400*	400
15 - 20°	Snow	Plow & apply chemical	200 – 280	175 – 250	250 – 350*	Not recommended
	Frz. rain	Apply chemical	240 – 320	210 – 280	300 – 400*	400
15 - 20°	Snow or Frz. rain	Plow & apply chemical	240 – 320	210 – 280	300 – 400*	500 for frz. rain
0 to 15~	Snow	Plow, treat with blends, sand hazardous	Not recommended	300 – 400	Not recommended	500 – 750 spot treat as needed
< 0~	Snow	Plow, treat with blends, sand hazardous	Not recommended	400 – 600**	Not recommended	500 – 750 spot treat as needed

*Dry salt is not recommended. It is likely to blow off the road before it melts ice. **A blend of 6 – 8 gal/ton $MgCl_2$ or $CaCl_2$ added to NaCl can melt ice as low as -10~.

Chapter 4
INTRODUCTION TO SLIP VARIABLES AND PIEZOELECTRIC SENSORS

This part of the report investigates the use of piezoelectric sensors to estimate the tire slip angle and the tire-road friction coefficient. The slip angle is defined as the angle between the orientation of the tire and the orientation of the velocity vector of the wheel (see Figure 4.1).

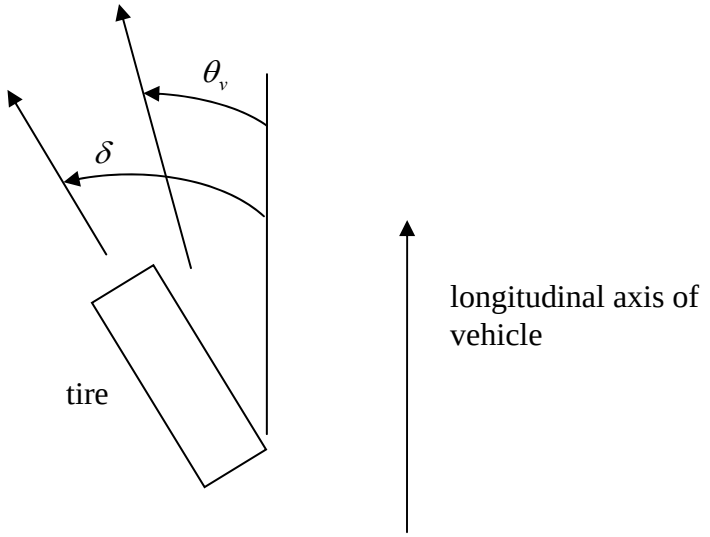

Figure 4.1 Tire slip angle [3]

δ represents the orientation of the tire (steering angle) and θ_v represents the orientation of the velocity vector. Hence the slip angle (α) is

$$\alpha = \delta - \theta_v \tag{4.1}$$

The friction coefficient is defined as the ratio of the maximum force available to the tires from the ground and the vertical force on the tires. If the lateral, longitudinal and vertical forces acting on the tire are F_x, F_y and F_z respectively, then the force acting on the tire from the ground is

$$F_g = \sqrt{F_x^{\,2} + F_y^{\,2}} \tag{4.2}$$

The friction coefficient μ is defined as

$$\mu = \frac{\max(F_g)}{F_z} \tag{4.3}$$

These two parameters are of significant importance in the development of different active safety systems on vehicles.

4.1 Motivation for estimation of slip angle and friction coefficient

There are various factors that determine the vehicle motion, namely driver input, road conditions, lateral and longitudinal tire forces etc. The forces from the tires that act on a vehicle during cornering are called lateral forces and are a function of slip angle, friction coefficient, tire cornering stiffness, vertical load and tire width. Estimation of lateral forces is an important factor in the study of vehicle dynamics for estimating vehicle motion accurately and reliably [1,2,9]. It is also important from the stand point of development of effective active safety systems like ABS, traction control systems, skid control systems etc [1,2,9]. While other parameters like the tire stiffness, width, vertical load are more or less constant, slip angle and friction coefficient are subject to change depending on driver input and road conditions. Therefore real time estimation of slip angle and friction coefficient is an important topic of research.

The measurement of tire-road friction coefficient is also useful for winter maintenance vehicles like snowplows [5]. These vehicles operate in a harsh winter road environment and the knowledge of friction coefficient can help improve the safety of operation. Further these vehicles need to apply anti-icing and deicing material to the roadway. The amount of deicing material depends on the amount of snow or ice present on the road. The presence of snow or ice tends to lower the tire-road friction coefficient. Therefore information on the friction coefficient can be used by the vehicle operator to adjust the amount and kind of deicing material to be applied to the roadway. It can also be used to automate this process.

4.2 Current Approaches

Most of the current approaches used to estimate slip angle use an indirect measurement to estimate the slip angle. For example the slip angle can be approximated based on the lateral and longitudinal velocity and the yaw rate of the vehicle [3]. Equation 4.4-4.6 show these relations

$$\alpha = \delta - \theta_V \tag{4.4}$$

where

α is the slip angle

δ is the tire steering angle

θ_V is the tire velocity angle

For the front and rear tire θ_{Vf} and θ_{Vr} are defined as

$$\theta_{Vf} = \frac{V_y + l_1 \dot{\psi}}{V_x} \tag{4.5}$$

$$\theta_{Vr} = \frac{V_y - l_2 \dot{\psi}}{V_x} \tag{4.6}$$

where

V_y is the lateral speed of the vehicle

V_x is the longitudinal speed of the vehicle

$\dot{\psi}$ is the yaw rate of the vehicle

l_1 and l_2 are the distance of the front and rear tire respectively from the c.g. of the vehicle.

Estimation of lateral velocity requires a two antenna and a very accurate differential GPS, which is extremely expensive and not suitable for production vehicle applications. Another approach is to use an accelerometer to measure lateral acceleration and integrate it to get lateral velocity. However this would create a bias in the estimation of lateral velocity which would have to be corrected using a GPS. However such a method is not reliable and it requires constantly correcting for the bias. There are other kinds of sensors like the CORREVIT SF optical sensor for tire-slip angle measurement, but are extremely expensive (about $30K) for commercial applications.

The existing approaches to friction measurement use either a vehicle based system or a redundant wheel based system.

a) Vehicle based system: - Vehicle based systems are typically based on calculating the longitudinal or lateral tractive force and using the relationship between the tractive force and slip angle or ratio to classify the surface [4,5]. For example in [5] the tractive force is calculated using an accelerometer and differential GPS. The normalized tractive force is calculated from the ratio of the tractive force and the vertical force on the tires. The longitudinal slip ratio is calculated using absolute vehicle speed from DGPS and wheel speed sensors from the ABS system. The limitation of the vehicle based system is that it cannot provide estimation of friction coefficient if the slip and slip angle are both very small. Therefore sufficient acceleration, deceleration or cornering is required for this method to work.

b) Redundant wheel based system: - This measurement system utilizes a redundant wheel mounted on the vehicle. Existing commercial friction measurements systems such as the Norse meter depend on the use of an additional wheel (an automobile tire) attached to the truck. This tire is automatically skidded on the roadway surface at timed intervals (and at the operator's discretion) and a friction value is recorded by the Norse meter.

4.3 Introduction to Piezoelectric Sensors

Piezoelectricity, Greek for "pressure" electricity, was discovered by the Curie brothers more than 100 years ago. They found that quartz changed its dimensions when subject to an electrical field, and conversely, generated electrical charge when mechanically deformed. In 1969, Kawai found very high piezo-activity in the polarized fluoropolymer, polyvinylidene fluoride (PVDF). Today, piezoelectric polymer sensors are among the fastest growing of the technologies within the world wide sensor market [6].

4.4 Piezo characteristics

(i) Mechanical to Electrical conversion

Piezo films possess high sensitivity as a receiver to mechanical work input. Like water from a sponge, piezoelectric materials generate charge when squeezed. In its simplest mode the film behaves like a dynamic strain gage except that it requires no external power source and generates signals greater than those from conventional foil strain gages after amplification. The extreme sensitivity is largely due to the format of the piezo film material. The low thickness of the film makes, in turn, a very small cross-sectional area and thus relatively small longitudinal forces create very large stresses within the material.

The amplitude and frequency of the signal is directly proportional to the mechanical deformation of the piezoelectric material. The resulting deformation causes a change in the surface charge density of the material so that a voltage appears between the electrode surfaces. Piezoelectric materials are not suitable for static measurements. The electric charges developed by piezo film decay with a time constant that is determined by the dielectric constant and the internal resistance of the film, as well as the input impedance of the interface electronics to which the film is connected. This has been discussed in detail in the next section.

The open-circuit output voltage for a piezo sensor is given by

$$V_0 = g_{3n} X_n t \tag{4.7}$$

where

n = 1, 2 or 3

g = appropriate piezoelectric coefficient for the axis of applied stress or strain

X_n = applied stress in the relevant direction

t = film thickness

(ii) Equivalent Circuit of Piezo Film

There are two valid models – one is a voltage source in series with a capacitance, the other is a charge generator in parallel with a capacitance. The former is commonly used in electrical circuit analysis. Figure 4.2 shows the piezo film as a simple voltage generator. The dashed line represents the “contents” of the piezo film. The voltage source V_S is the piezoelectric generator itself, and this source is directly proportional to the applied stimulus (pressure, stress, strain etc.). It is important to note that this voltage source will absolutely follow the applied stimulus, i.e. it is a “perfect” source. However the node marked “X” can never be accessed.

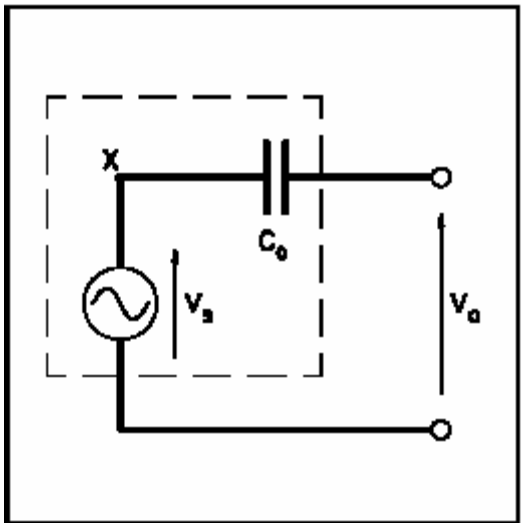

Figure 4.2 Piezo film element as a simple voltage generator

(iii) Effect of adding a resistive load

The effect of connecting the piezo to an oscilloscope or other data acquisition devices, used to read the voltage output, can be analyzed by modeling the oscilloscope simply as a pure resistance, and neglecting the very small capacitance associated with the cables, in comparison to the film capacitance. Figure 4.3 shows the circuit diagram of a piezo connected to a resistive load.

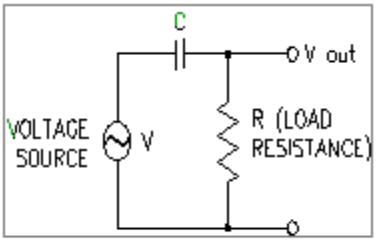

Figure 4.3 Piezo connected to a resistive load

The voltage measured across the load resistor R_L will not necessarily be the same voltage developed by V_S. The proportion V_L of V_S which appears across R_L is given by:

$$\frac{V_L(s)}{V_S(s)} = \frac{s}{s + 1/(R_L C_0)} = G(s) \tag{4.8}$$

This transfer function acts as a high pass filter. The quantity $R_L C_0$ is the time constant, and $1/(2\pi R_L C_0)$ is called the cut-off frequency. If we want the measured voltage (V_L) to be proportional to the developed voltage (V_S), we need to make the time constant very small.

This can be achieved by increasing the value of R_L, or by connecting an external capacitor C_E in parallel across R_L. In this case the above equation will change to:

$$\frac{V_L(s)}{V_S(s)} = \frac{sR_L C_0}{1 + sR_L(C_0 + C_E)} \tag{4.9}$$

In this case the time constant is given by

$$\tau = R_L(C_0 + C_E) \tag{4.10}$$

and the cut-off frequency is given by

$$\omega_C = \frac{1}{2\pi R_L(C_0 + C_E)} \tag{4.11}$$

Hence if a large enough value of R_L and C_E, then we can ensure that the measured voltage will be proportional to the applied stimulus. Piezoelectric sensors are usually suitable for frequencies above 0.001 Hz and not for pure d.c. inputs.

Chapter 5

TIRE MODELS

This chapter discusses some of the commonly used tire models and the underlying assumptions for the development of such models. Tire models are used to calculate the tire forces and moments as responses to the relative wheel motion with respect to the ground. They also give the relation between tire deflections and parameters like slip angle and friction coefficient. The piezoelectric theory discussed in the previous chapter that relates piezo deflections to the voltage produced by these sensors and the theory from these tire models together form the basis of the method used for estimating tire-road friction coefficient and slip angle. This has been discussed in detail in chapter 7.

There are theoretical tire models based on the physics of the tire tread deflections, and empirical models which are solely based on data from experimental findings. Both these kinds of models are discussed in this chapter and the relation between the theoretical and experimental models is also presented.

5.1 Generation of Lateral Forces

Lateral forces on the tire from the road occur primarily due to the presence of side-slip angles i.e. due to the velocity of the tire being at an angle to the orientation of the tire [8-10]. Or in other words due to the presence of non-zero lateral velocity. Friction forces act in a direction opposite to that of the velocity. The friction forces between the tire and the road cause lateral deformation of the tire. The lateral force generated depends on the slip angle, the friction coefficient and the vertical load.

There are three principal models used to understand lateral tire forces and deflections during cornering: the elastic foundation or the brush model, the string model and the beam on elastic foundation.

In the elastic foundation model, each small element of the contact patch surface is considered to act independently. Each element is constrained by a foundation stiffness spring; if forced by the ground it can be displaced from its null position relative to the foundation. The foundation stiffness model allows a discontinuous distribution of displacement and slope of the center-line.

In the string model, lateral displacement of each element is also resisted by tension between the elements, because of changes in the displacement slope. The string model allows discontinuous change of slope, but not of deflection.

In the beam model the tread is considered equivalent to an elastic beam with continuous lateral elastic support. The beam model does not allow discontinuities of either displacement or slope. Figure 5.1 shows pictorially the string and the beam model [7].

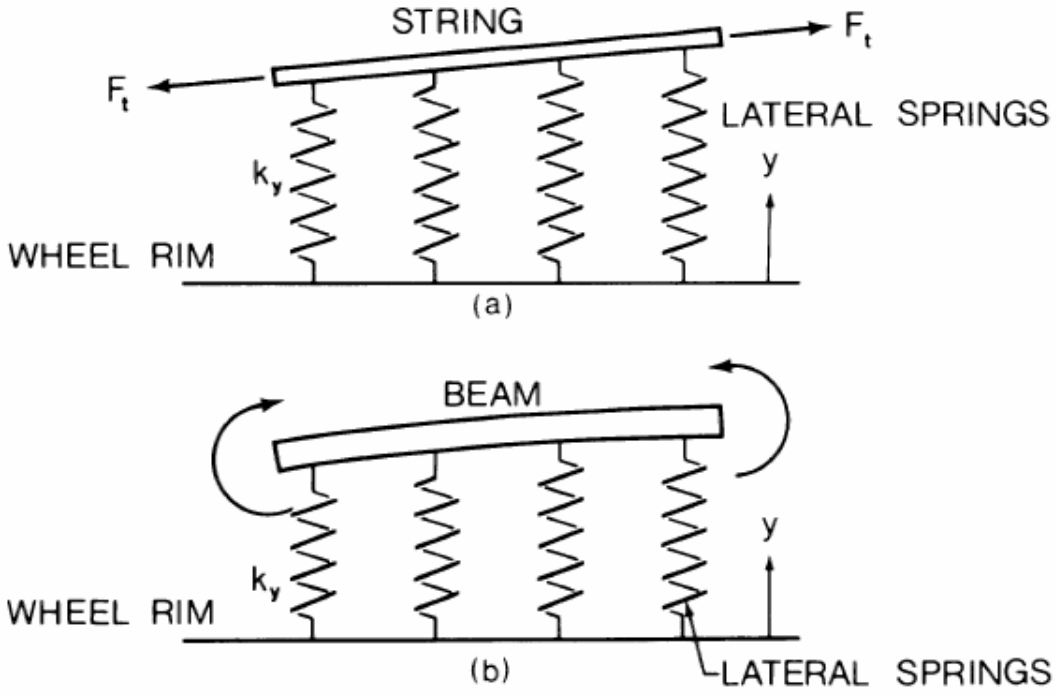

Figure 5.1 (a) String model, (b) Beam on elastic foundation model [7]

The next section discusses the relations obtained using the elastic foundation model. The elastic foundation model, is the simplest, but still produces many of the interesting characteristics of a real tire.

5.2 Elastic Foundation or Brush Model

Figure 5.2 shows a plan view of a tire during cornering, showing the lateral deflection of the tire center-line in the contact patch [8-10].

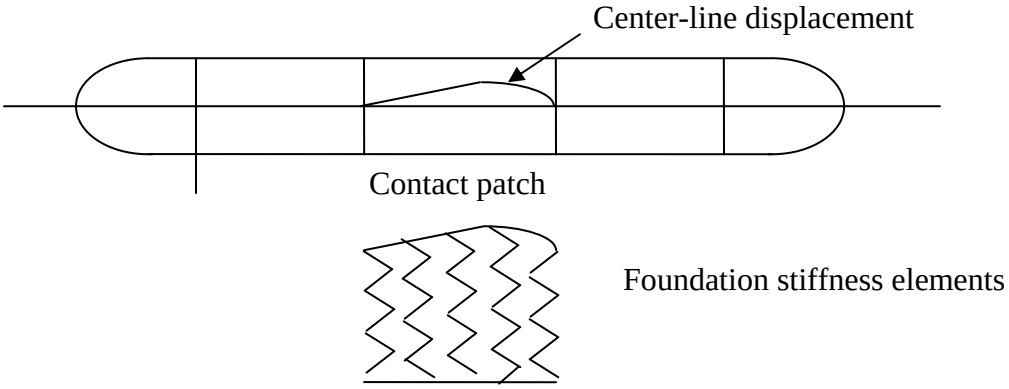

Figure 5.2 Plan view of a tire during cornering

The lateral deflection profile for the tire center-line depends on the pressure distribution assumption in the contact patch. The pressure distribution can be assumed to be constant or parabolic. Both these cases are discussed below.

5.2.1 Lateral Forces under Uniform Contact Pressure assumption

If we assume a uniform contact pressure, then

$$p(x) = \frac{F_z}{(2a)(2b)} \tag{5.1}$$

where $2a$ is the contact patch length and $2b$ is the tire width

The lateral force at the beginning of the contact patch will be zero and will increase linearly till it attains the maximum value and will then saturate. The maximum value that the friction force can reach is μF_z (Equation 4.3). The point of saturation will depend on the slip angle (as shown in Figure 5.3). If the slip angle is large enough then the point of saturation can be less than $2a$. Since in the elastic foundation model each element is constrained by just a spring, hence the tire center-line deflection will have the same profile as the lateral force. Figure 5.3 shows the lateral force and the corresponding lateral deflection of a tire for two different slip angles α_1 and α_2.

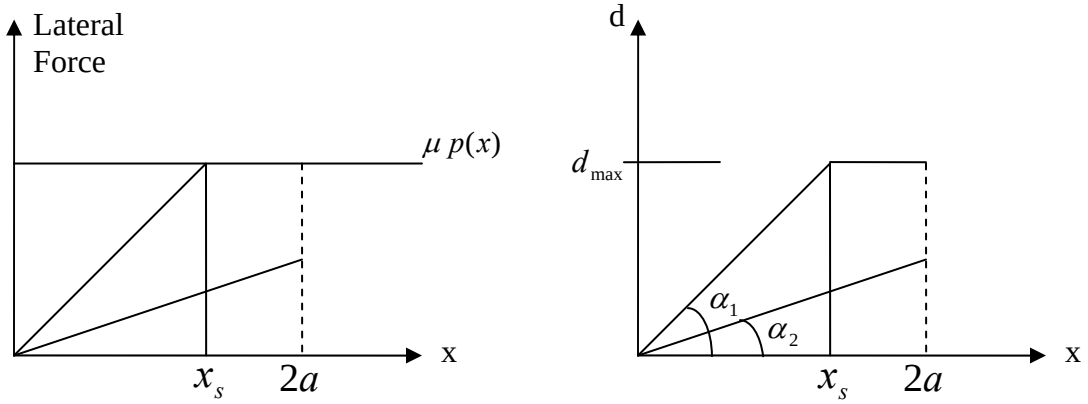

Figure 5.3 Plots showing lateral force and lateral tire deflection along the contact patch for different values of slip angle

If c is the lateral stiffness per unit length of the tire and d(x) the lateral displacement of the tire as a function of x, then it can be said that there will be no sliding if,

$$cd(x) \le \frac{\mu F_z}{2a} \tag{5.2}$$

along the entire contact patch.
Hence maximum possible lateral displacement with no sliding is

$$d_{\max} = \frac{\mu F_z}{c(2a)} \tag{3.3}$$

In the presence of sliding lateral slip is defined as

$$S = \tan(\alpha) = \frac{d_{\max}}{x_s} \tag{5.4}$$

where x_s is the point of initiation of sliding (Figure 5.3)

Therefore

$$x_s = \frac{d_{\max}}{S} = \frac{\mu F_z}{2acS} \tag{5.5}$$

$$\Rightarrow \mu = \frac{(2acS)x_s}{F_z} \tag{5.6}$$

So if the slip angle (α), vertical force (F_z), length of contact patch ($2a$), lateral stiffness per unit length (c) and the point of initiation of sliding (x_s) are known the friction coefficient can be calculated.

5.2.2 *Lateral Forces under Parabolic Pressure Distribution*

A parabolic pressure distribution along the contact patch is given by

$$p = p_0\left\{1 - \frac{w^2}{a^2}\right\} \tag{5.7}$$

Figure 5.4 shows a typical contact patch

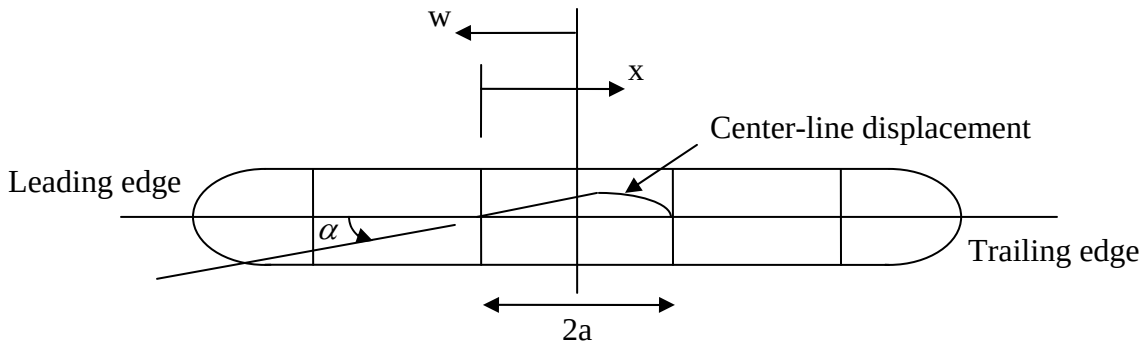

Contact patch

Figure 5.4 Tire deformation under parabolic pressure distribution

Vertical force equilibrium using $\int_{-a}^{a} 2bp(w)dw = F_z$ gives

$$p_0 = \frac{3F_z}{8ab} \tag{5.8}$$

Hence

$$p(x) = \frac{3F_z}{8ab}\left[1 - \frac{(a-x)^2}{a^2}\right] \tag{5.9}$$

The lateral force per unit length will increase linearly from zero till the point when it intersects the available lateral force distribution. The point of intersection is the point of initiation of sliding and will depend on the slip angle α. Again as in the previous case, the tire centerline deflection will have the same profile as the lateral force. Figure 5.5 shows the lateral force and lateral tire deflection along the contact patch.

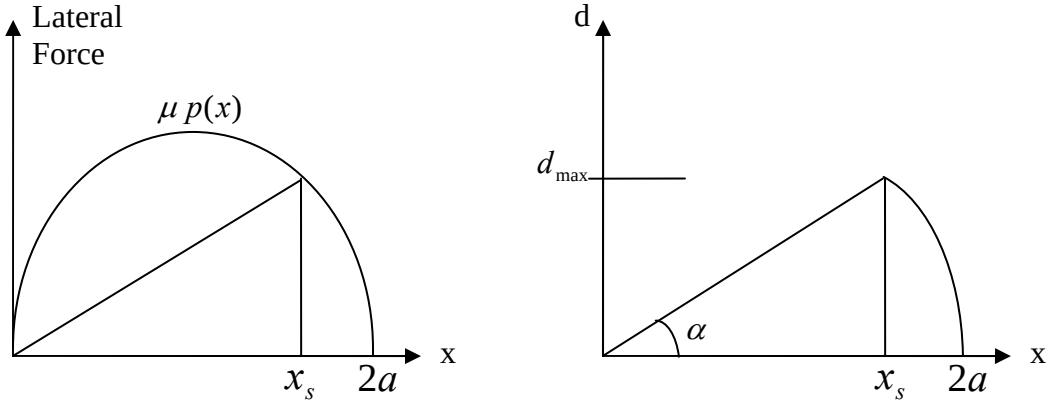

Figure 5.5 Lateral force and lateral tire deflection along the contact patch for parabolic pressure distribution

It is important to note that if α is large enough then it is possible to have $x_s < a$. In that case $x_{\max} = a$, irrespective of α.

So in general it can be said that

$$kd_{sliding}(x) = \mu p(x) \tag{5.10}$$

$$kd_{sliding}(x) = \frac{3\mu F_z}{8a^3 b}\{x(2a-x)\} \tag{5.11}$$

Define $\theta = \dfrac{4a^2 bk}{3\mu F_z}$

Hence,
$$d_{sliding}(x) = \frac{1}{2a\theta}\{x(2a-x)\} \tag{5.12}$$

For initiation of sliding we must have

$$kd(x_s) = \mu p(x_s) \tag{5.13}$$

$$kd(x_s) = kd_{sliding}(x_s) \tag{5.14}$$

$$\Rightarrow Sx_s = \frac{1}{2a\theta}\{x_s(2a-x_s)\} \tag{5.15}$$

where $S = \tan(\alpha)$

Hence

$$x_s = 2a(1-\theta S) \tag{5.16}$$

Therefore if the slip angle (α), vertical force (F_z), length of contact patch ($2a$), lateral stiffness per unit length (c) and the point of initiation of sliding (x_s) are known the friction coefficient can be calculated.

5.3 Beam on Elastic Foundation model

Ellis (1969) [11] had proposed two analytical models for tire lateral response: the string model and the beam on elastic foundation. The mathematical derivation for Ellis' elastic beam model uses several numerical approximations and he treats tread and sidewall deflections separately. In this model the tire is treated as a beam restrained by an elastic foundation attached to a fixed base (wheel rim). Beam deflection represents tire tread lateral deflections, which follow a linear path in the static region of the contact patch determined by the slip angle α, and a parabolic curve in the sliding region (Figure 5.6)

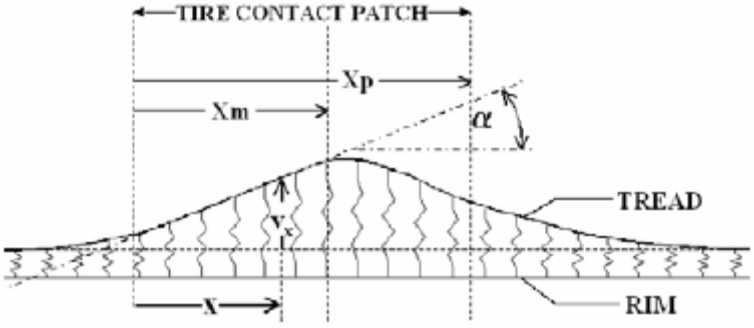

Figure 5.6 Plan view of Tire Patch Lateral Deflection using a Beam on Elastic Foundation Model [11]

For further details on the beam model the reader is referred to Lacombe, James 2000, Tire model for simulations of vehicle motion on high and low friction road surfaces, Proceedings of the 2000 Winter Simulation Conference.

A simplified form of the beam model is assumed here, with a linear static region and a parabolic sliding region as shown in Figure 5.7. This model will be used later in chapter 5 for analyzing the piezo signals.

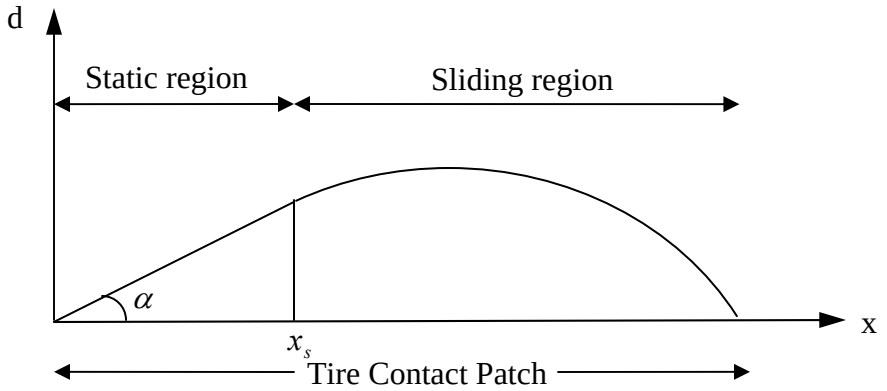

Figure 5.7 Simplified form of the beam model

A major difference to note about the beam model is that there is continuity in slope at point x_s, unlike the elastic foundation model.

5.3.1 Equation for the parabolic curve

The deflection profile in the beam model consists of a linear region and a parabolic region. The equation for the linear region is given by

$$y_1 = \tan(\alpha)x \tag{5.17}$$

Let the equation for the parabolic region be given by

$$y_2 = a_1x^2 + a_2x + a_3 \tag{5.18}$$

We have the following boundary conditions for the parabolic curve

1) $x = 2a, y_2 = 0$
2) $x = x_s, y_2 = \tan(\alpha)x_s$
3) $x = x_s, \frac{dy_2}{dx} = \tan(\alpha)$

Using the above conditions we get

(i) $$a_1 = \frac{-\tan(\alpha)(2a)}{(x_s - 2a)^2} \tag{5.19}$$

(ii) $$a_2 = \frac{(x_s{}^2 + (2a)^2)(\tan(\alpha))}{(x_s - 2a)^2} \tag{5.20}$$

(iii) $$a_3 = \frac{-\tan(\alpha)(2a)(x_s{}^2)}{(x_s - 2a)^2} \tag{5.21}$$

Also the peak deflection in this case will always occur in the parabolic region. The length along the contact patch where this peak will occur is given by

$$x_{\max} = \frac{dy_2}{dx} = 0$$

$$= \frac{-a_2}{2a_1}$$

$$= \frac{x_s^{\,2} + (2a)^2}{2(2a)}$$

Therefore

$$x_s = \sqrt{2(2a)x_{\max} - (2a)^2} \tag{5.22}$$

Also if $x_s = 0$, then $x_{\max} = a$. Therefore the peak can occur only for $a \le x \le 2a$.

Hence if the peak value is known then the point of initiation of sliding i.e. x_s can be calculated.

For initiation of sliding we must have

$$kd(x_s) = \mu p(x_s) \tag{5.23}$$

which again gives

$$x_s = 2a(1 - \theta S) \tag{5.24}$$

where $\theta = \dfrac{4a^2 bk}{3\mu F_z}$

Hence if x_s is known the coefficient of friction i.e. μ can be calculated.

5.4 Magic Formula Tire Model

Magic formula [12] is a widely used empirical tire model that was developed in the mid eighties. The magic formula tire model reads:

$$y = D\sin[C\tan^{-1}\{Bx - E(Bx - \tan^{-1}(Bx)\}] \tag{5.25}$$

with

$$Y(x) = y(x) + S_v$$

$$x = X + S_h$$

where

Y : output variable F_y

X : output variable α

with

B: stiffness factor

C: shape factor

D: peak value

E: curvature factor

S_h : horizontal shift

S_v: vertical shift

The variables B, C, D and E are functions of the wheel load, slip angle, slip ratio and camber.

$$C = \frac{2}{\pi}\sin^{-1}\left(\frac{y_a}{D}\right) \text{ and } E = \frac{Bx_m - \tan(\pi/2C)}{Bx_m - \tan^{-1}(Bx_m)}$$

Figure 5.8 shows the curve produced by the Magic formula.

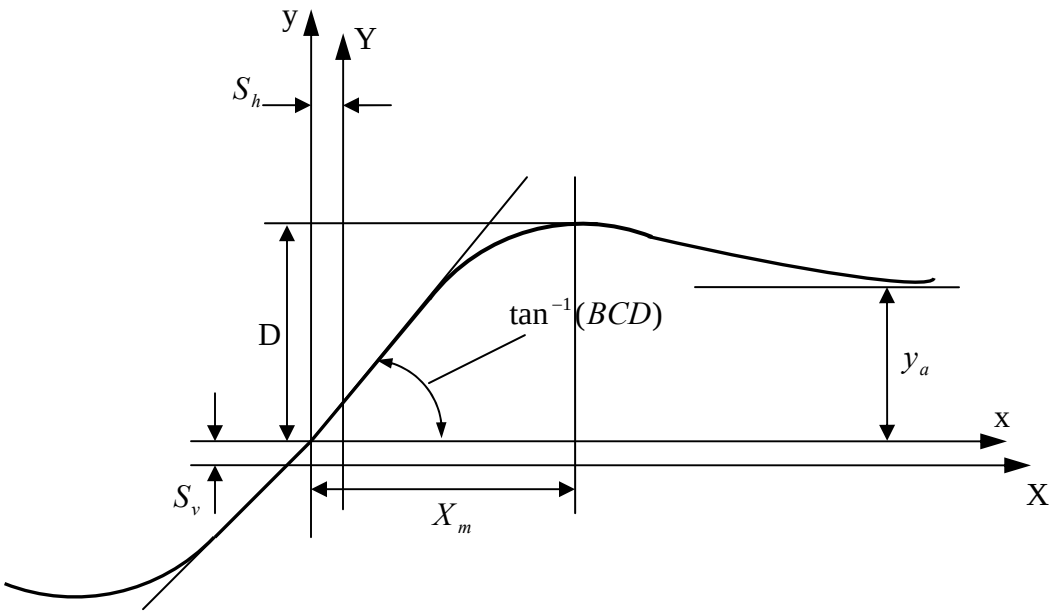

Figure 5.8 Curve produced by the Magic Formula, Equation (5.25)

5.5 Relation between Magic Formula and Elastic Foundation Model

The magic formula for $y(x)$ typically produces a curve that passes through the origin $x = y = 0$, reaches a maximum and subsequently tends to a horizontal asymptote (refer to Figure 5.8). If the output variable is the lateral force and the input variable is the slip angle, then the magic formula tire model illustrates that the lateral tire force increases linearly with slip angle and then saturates after reaching an intermediate peak value. The saturation value is less than the peak value.

The lateral force for a particular value of slip angle as given by the elastic foundation model (section 5.2.1 and 5.2.2) is proportional to the area of the lateral deflection profile. If the slip angle is varied and the lateral force is calculated for each setting of slip angle, then it can be observed that the force would increase and then saturate. A peak value won't be obtained for the lateral force. In other words the saturation value will be equal to the peak value.

Figure 5.9 shows the lateral tire deflection for increasing values of α under the uniform and parabolic pressure distribution assumption. As can be seen the area under each profile will continuously increase with α .

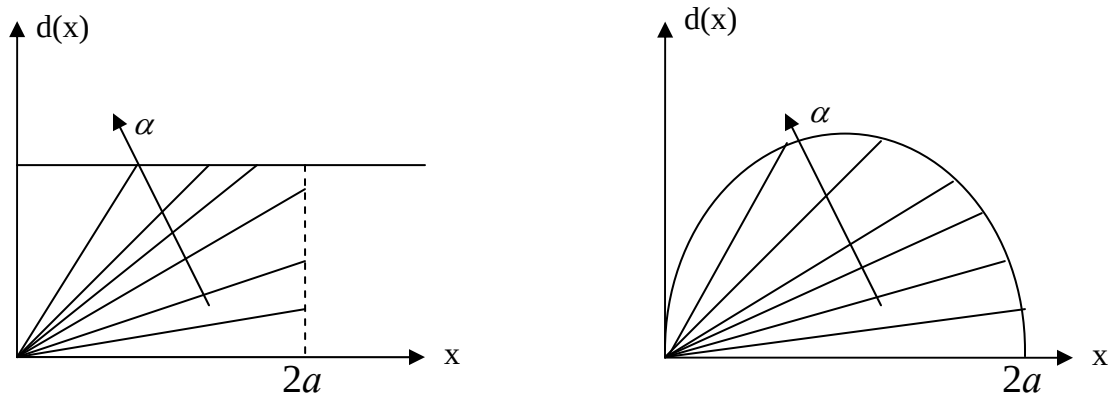

Figure 5.9 Plots showing the lateral tire deflections for increasing values of slip angles

This behavior is inconsistent with the magic formula tire model which has been verified experimentally. However the elastic foundation model can be modified to address this issue. In the elastic foundation model each element of the tire in the contact patch was considered as a spring acting independently under the influence of lateral force. The lateral force for a particular value of slip angle was assumed to increase linearly causing the tire elements to deflect and then force would saturate to the maximum available lateral force causing the tire elements to slide. Here it was assumed that the maximum available lateral force in the static and sliding region is the same. Or in other words the coefficients of kinetic (sliding) and static friction were assumed to be same.

However the friction coefficient depends on the sliding speed. According to the classical Coulomb friction model, for sliding speed = 0 the coefficient of friction is $\mu = \mu_s$. For sliding speed > 0, the coefficient of friction is $\mu = \mu_k$. There are four commonly used analytic friction-speed models used to approximate this piecewise continuous friction profile [13]:

(1) Constant μ ($\mu_s = \mu_k$)

(2) Different static and dynamic values μ_s and μ_k

(3) $\mu_k = \mu_s(1 - KV)$

(4) $\mu_k = \mu_s e^{-V/V_1}$

where V is the sliding speed and V_1 and K are constants.

The second model assumes a step transition from μ_s to μ_k . Models 3 and 4 allow for a more smoother transition, assuming a linear and exponential decrease in the value of friction coefficient respectively.

Although more complex models are needed for accurate analysis, model (2) is sufficient to understand the relation between the magic formula and brush model, by defining one static coefficient of friction applicable the non-sliding part of the tire, plus a lower dynamic

coefficient of friction applicable to the sliding part of the tire. Figure 5.10 shows an illustration of the partition of contact area into regions of adhesion (non-sliding) and sliding and the lateral sliding forces in those regions. μ_s and μ_k represent the coefficient of static and kinetic friction respectively.

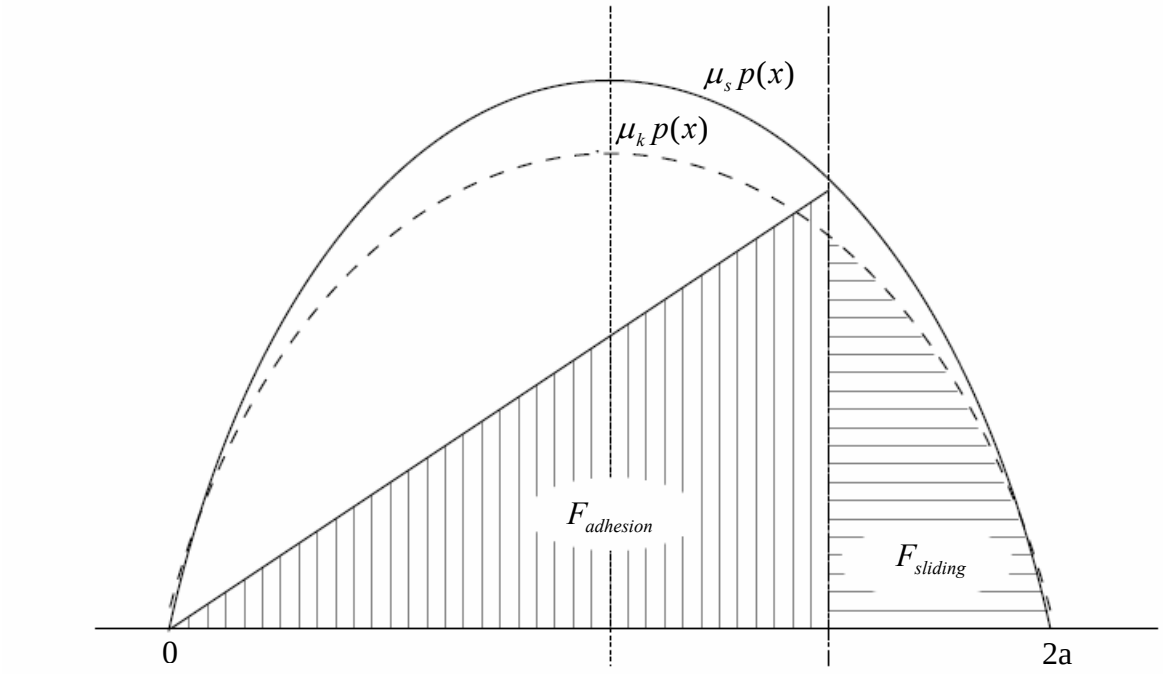

Figure 5.10 Illustration of partition of the contact patch into regions of adhesion and sliding [14]

The vertically and horizontally stripped areas represent the total forces of adhesion and sliding. Therefore the total available lateral force is given by

$$F_{total} = F_{adhesion} + F_{sliding} \tag{5.26}$$

If the total force is computed for different values of slip angles, and plotted as a function of the slip angle, it shows an initial increase with slip angle, reaches a maximum and then saturation, a behavior also shown by the magic formula. Figure 3.11 shows a hypothetical plot for lateral force vs. slip angle from such a computation, where the lateral force is computed by calculating the areas of the horizontally and vertically stripped areas.

Since the difference between the coefficient of static and kinetic friction is not significant, these two coefficients were not considered separately in the brush model. In the analysis presented in this thesis too they would be assumed to be equal.

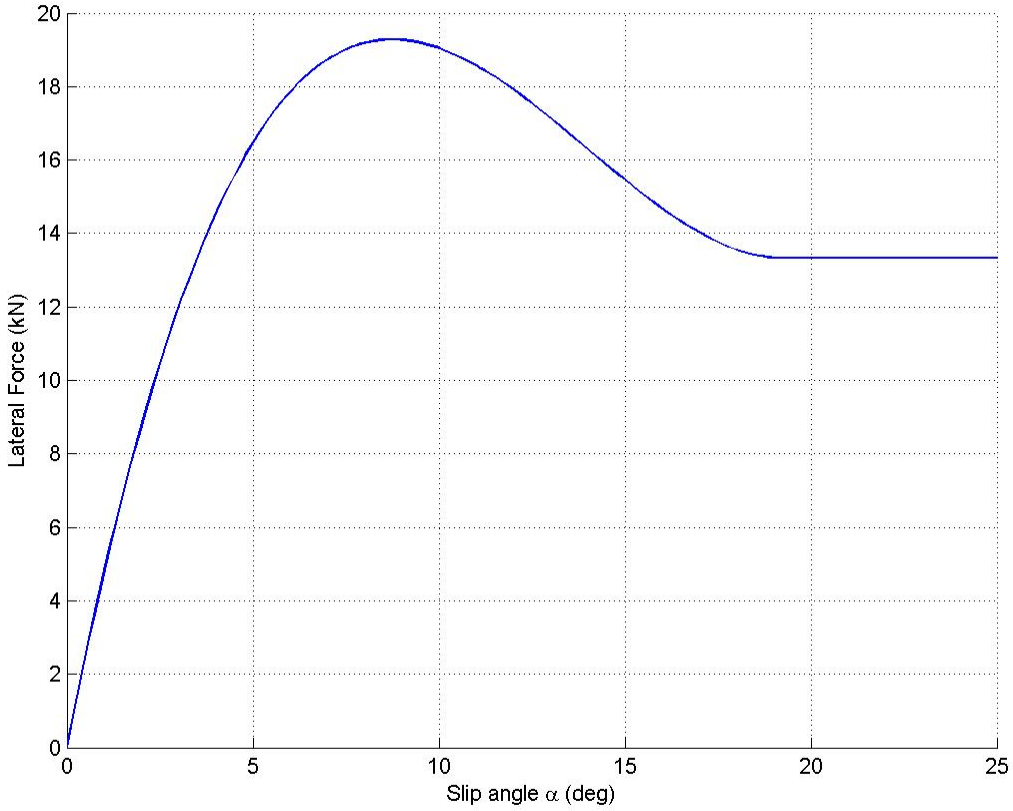

Figure 5.11 Plot showing variation of lateral force vs. slip angle

Chapter 6

EXPERIMENTAL SETUP

The theory on tire models shows that various parameters like slip angle and friction coefficient can be calculated if the deflection profile of the tire is known. Piezo sensors can be used to obtain this profile. These sensors, as was discussed earlier, generate a voltage proportional to applied stimulus, tire deflection in this case. Figure 6.1 shows the experimental setup used.

Figure 6.1 Photograph of the experimental setup

6.1 System Hardware

The sensors are mounted inside the extra wheel. This wheel is then set at an angle (slip angle) with respect to the scooter. Weights are placed to provide the desired vertical force. National Instrument's data acquisition card PCI-MIO-16E-4 and Matlab's real time software XPC were used to read out the voltage from the piezo sensors. Figure 6.2 shows the schematic diagram for the system hardware.

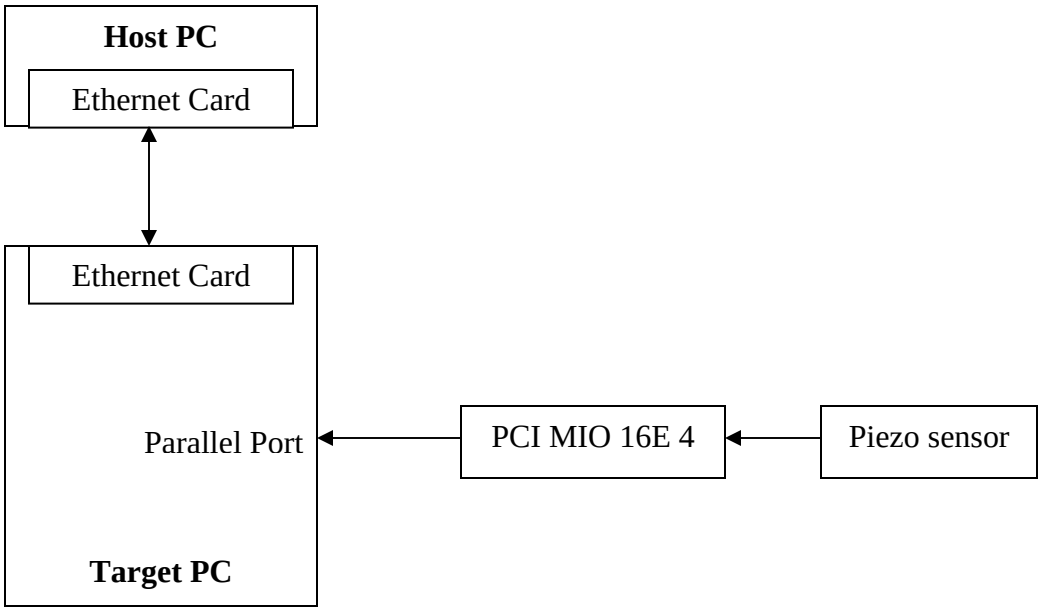

Figure 6.2 Schematic showing the organization of system hardware

6.2 Location of the extra wheel

An extra wheel was used instead of the actual wheels of the scooter for the experiments. The wheel was connected with the scooter through a link which could be rotated to set the wheel at the desired slip angle. Weights were placed on the link to provide the necessary vertical force. The extra wheel also provided for easy removal for putting the sensors and trying different configurations as discussed in the next section. Figure 6.3 shows a schematic of the front and top view of the link used to connect the extra wheel.

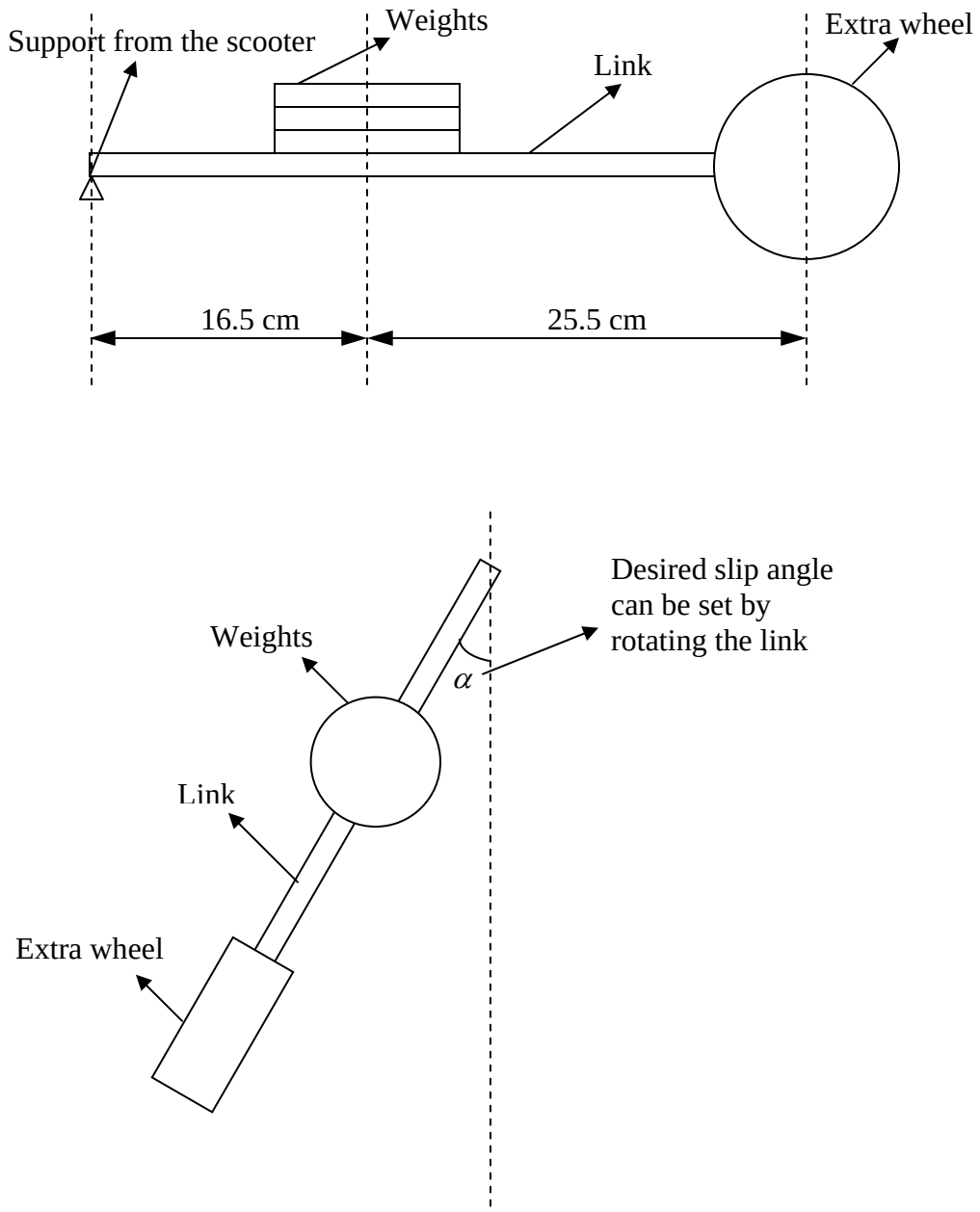

Figure 6.3 Front and top view of the experimental setup

Therefore if a weight 'W' is placed on the link, then the vertical force experienced by the extra wheel would be

$$R = \frac{16.5}{16.5 + 25.5} W \tag{6.1}$$

6.3 Location of the Piezo Sensors

The piezo sensors are extremely sensitive and hence it is important to figure out how to put these sensors on the tires. Initially the sensors were pasted on the outside of the sidewalls of

the tire. In this case the sensors were be affected by both the vertical and lateral force. Experiments were conducted for various slip angle values including zero. However since the magnitude of lateral force being generated was not enough, the side walls were not affected much by the lateral force. Hence the piezo sensor reading for different slip angle settings were almost identical.

Two approaches were tried out to eliminate the effect of the vertical load. This was done by putting the piezo inside the tire instead of the side walls, and designing a mechanism which will allow the piezo to move freely in the vertical direction, but constrain its movement in the lateral direction. Figure 6.4 and 6.5 show the methods tried out.

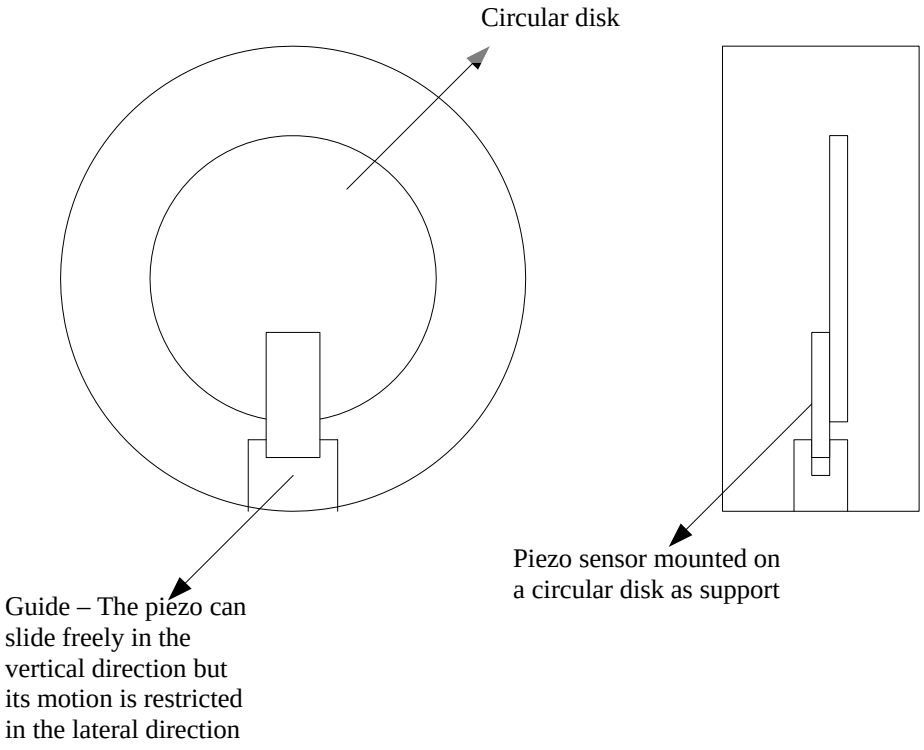

Figure 6.4 First method used to eliminate the effect of the vertical load

In this setup a piezo sensor was mounted on a circular disk, which was attached to the rim of the wheel. A wooden support with a slot was installed at the base of the tire. The slot acted as a guide for the piezo. This whole set up rotated with the tire. The purpose of this mechanism was to ensur that the piezo could slide freely in the vertical direction when it came into the contact patch, and hence be unaffected by the vertical force. However since its movement was constrained in the lateral direction, it would bend according to the lateral deflection of the tire, and hence would capture just the lateral deflection profile of the tire.

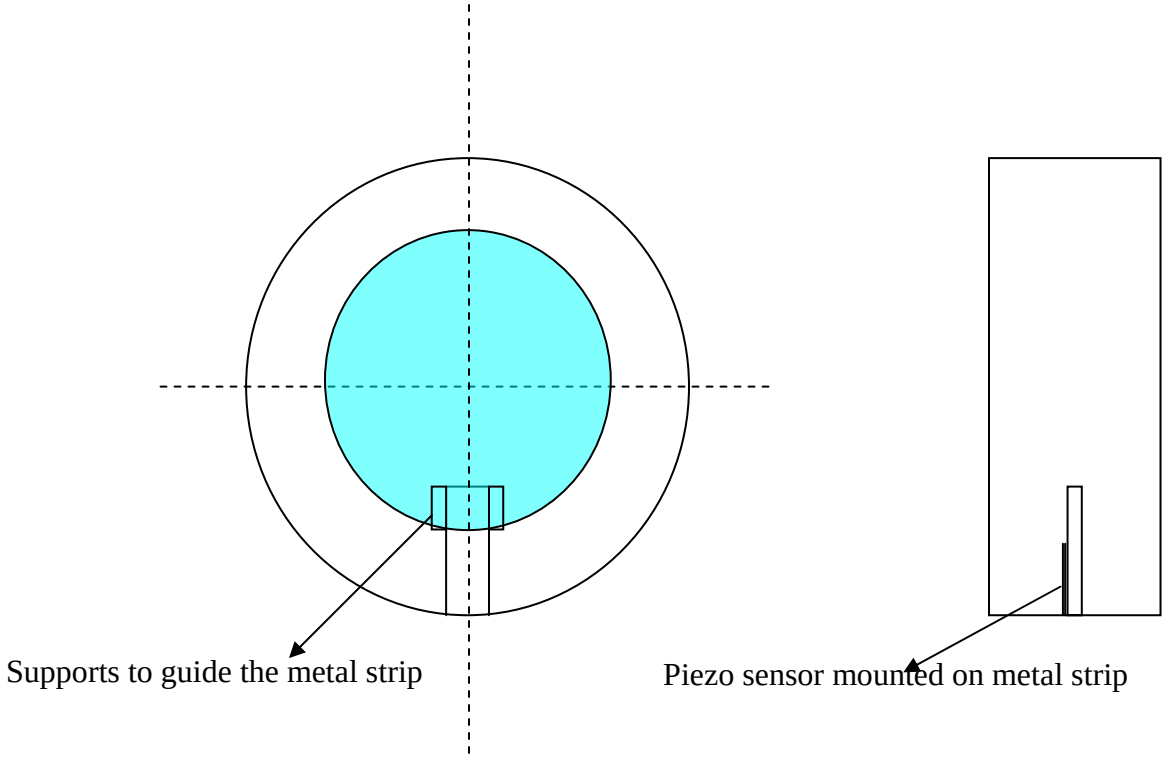

Figure 6.5 Second method used to eliminate the effect of the vertical load

This setup was designed to satisfy the same requirement i.e. to allow the piezo sensor to move freely in the vertical direction but to constrain its motion in the lateral direction. However in this method the piezo was mounted on a metal strip with its tip embedded in the tire. This was done to increase the sensitivity of the sensor as it was directly in contact with the tire. The metal strip was free to move in the vertical direction guided by two supports on the rim of the wheel.

However these mechanisms didn't produce the desired result i.e. they could not effectively eliminate the effect of the vertical load because it required the sensor to be precisely positioned at the center of the tire. It was not feasible to always ensure this condition as camber in the tire would cause the vertical load to shift away from the center of the tire.

Finally the approach adopted was to put the sensor inside the tire all the way to the tire centerline, as shown in Figure 6.6. Since the tip of the piezo was near the tire centerline, it ensured that the sensor would experience sufficient lateral force at different slip angles. However a different approach had to be used to separate the effects of the vertical and lateral forces on the sensor. This is discussed in the following chapter.

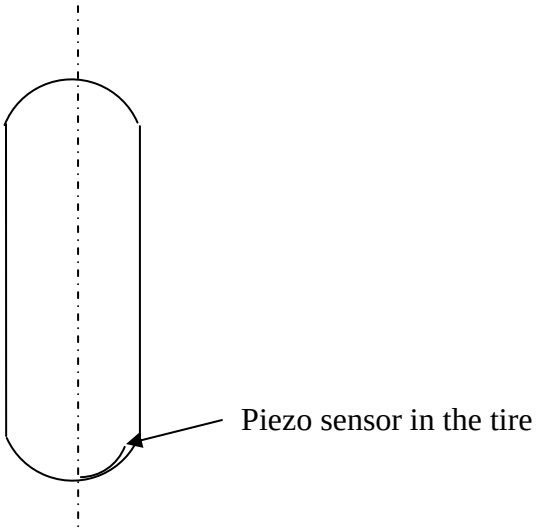

Figure 6.6 Schematic of the location of the piezo inside the tire

In this approach the piezo sensor was affected by both the vertical and lateral force. The stress developed in the piezo sensor would always be in the same direction because the direction of the vertical force will remain the same. However the lateral force can act from left to right or vice versa depending on the orientation of the tire with respect to the scooter. Therefore the lateral force could increase the overall stress or tend to reduce it.

Chapter 7

ANALYSIS OF SENSOR DATA

The voltage signal obtained from the piezo sensors is not continuous. The sensor experiences a stimulus only when it is in the contact patch. For the remaining part of the revolution of the tire, the piezo sensor provides no useful information. Hence the first step in analyzing the voltage signal is to determine the time period during which the sensor was in the contact patch. A typical piezo signal is shown in Figure 7.1. In this signal the piezo enters the contact patch at t = 3.85 sec and leaves the contact patch at t = 4.032 sec.

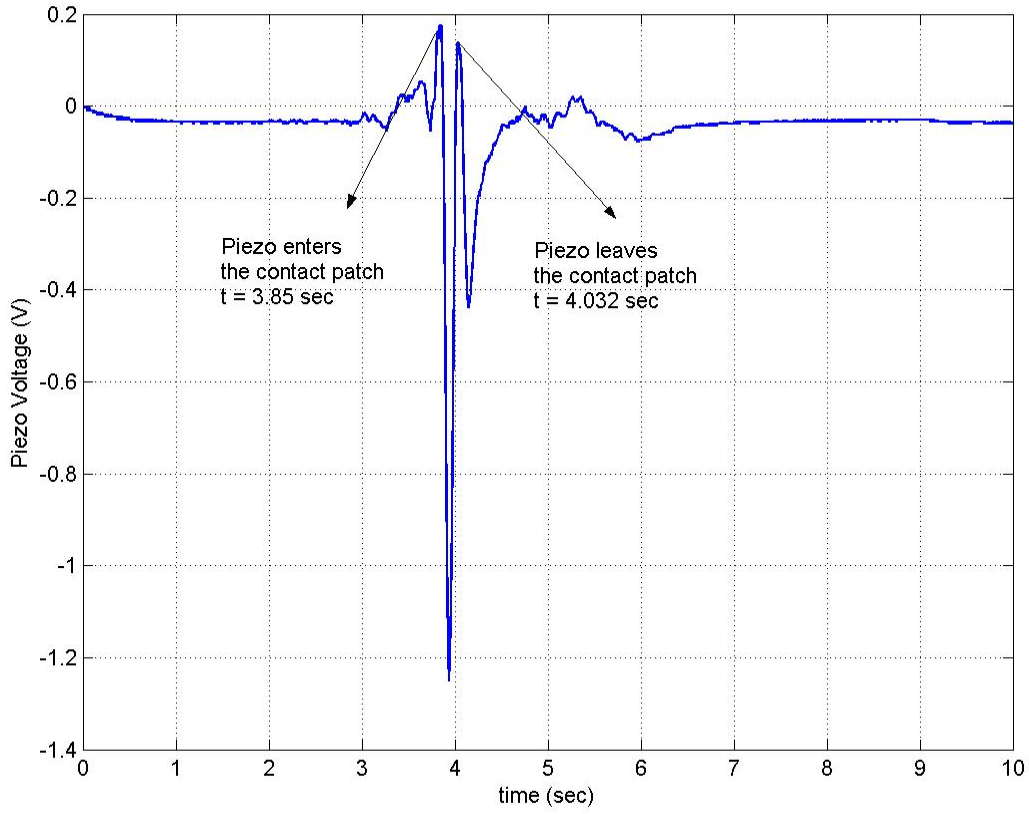

Figure 7.1 Plot showing a typical piezo signal

7.1 Extracting the signal

To extract the relevant portion of the signal, it is differentiated with respect to time to remove the bias and to get the points where the signal changes its slope. After differentiating the above signal we obtain the result as shown in Figure 7.2.

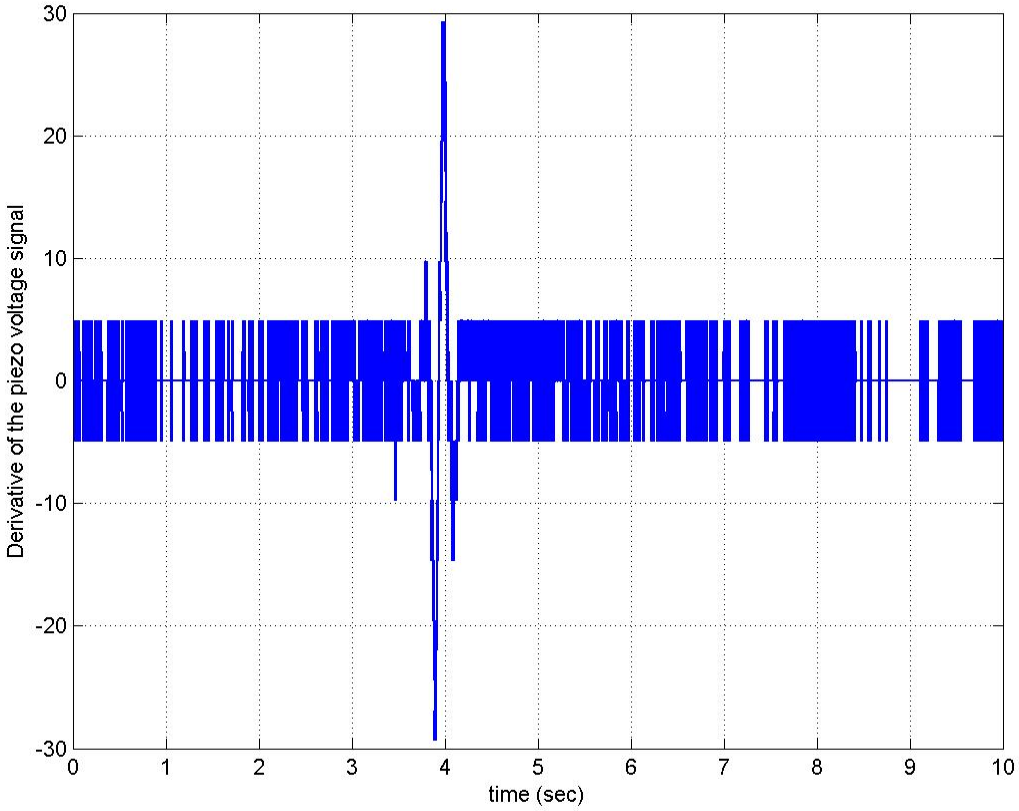

Figure 7.2 Plot showing the differentiated piezo signal

The resulting data has a lot of noise. To remove this noise this data is then passed through a median filter.

A low pass filter was not used because it only reduces noise, while a median filter completely removes noise above a certain frequency without affecting the signal. Figure 7.3 shows the result obtained by using the low pass filter $\frac{1}{0.01s+1}$ instead of the median filter.

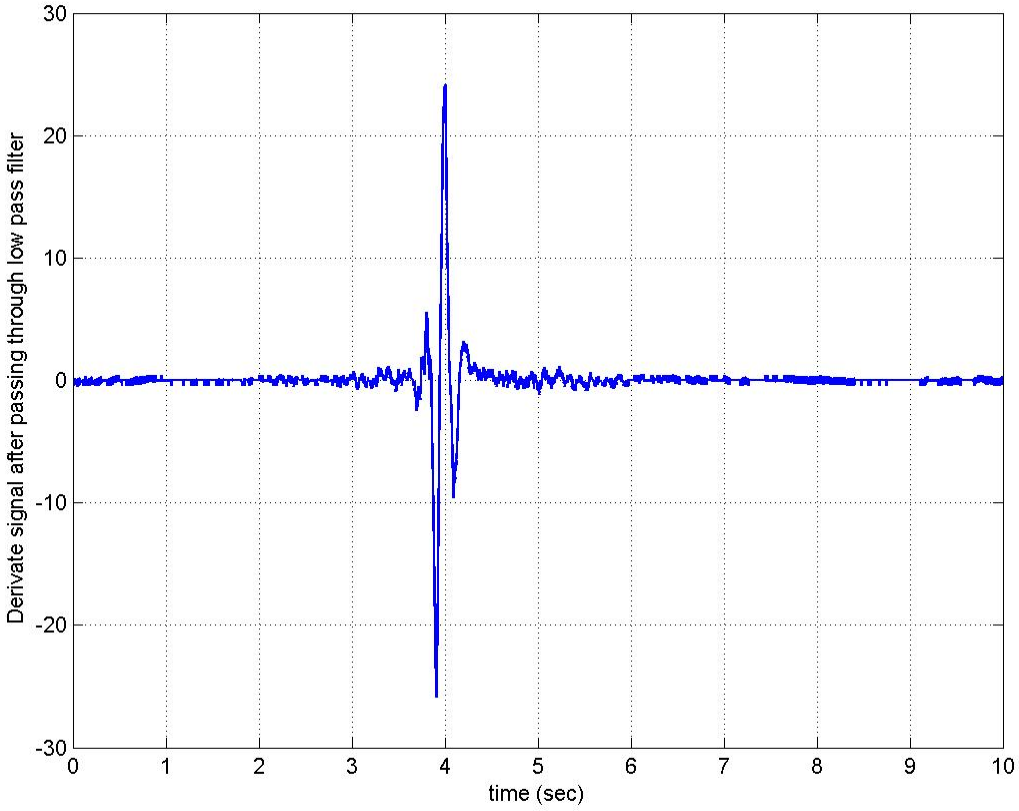

Figure 7.3 Plot showing the differentiated piezo signal after passing it through a low pass filter

7.1.1 Median Filter

Median filter is a non linear signal enhancement technique for smoothing the signals, the suppression of impulse noise, and preserving the edges. In the one-dimensional case it consists of sliding a window of an odd number of elements along the signal, replacing the center sample by the median of the samples in the window. A median filter of order 5 was chosen and the following result (Figure 7.4) was obtained after filtering the above data.

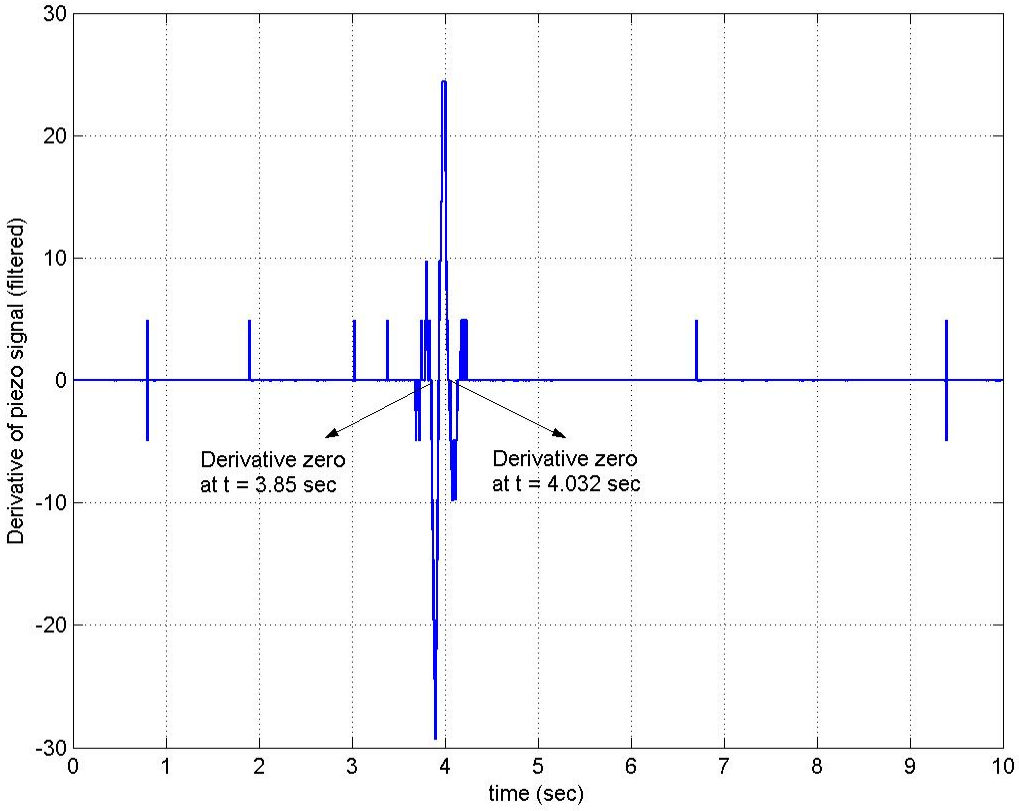

Figure 7.4 Plot showing the differentiated piezo signal after passing it through a median filter

After filtering, the time samples at which the derivative of the piezo voltage is zero around the peaks is determined, to get the time interval when the piezo sensor was in the contact patch of the tire. These time samples turn out to be t_1 = 3.851 and t_2 = 4.032. Figure 7.5 shows the plot of the piezo signal measured during the time period when it was in the contact patch.

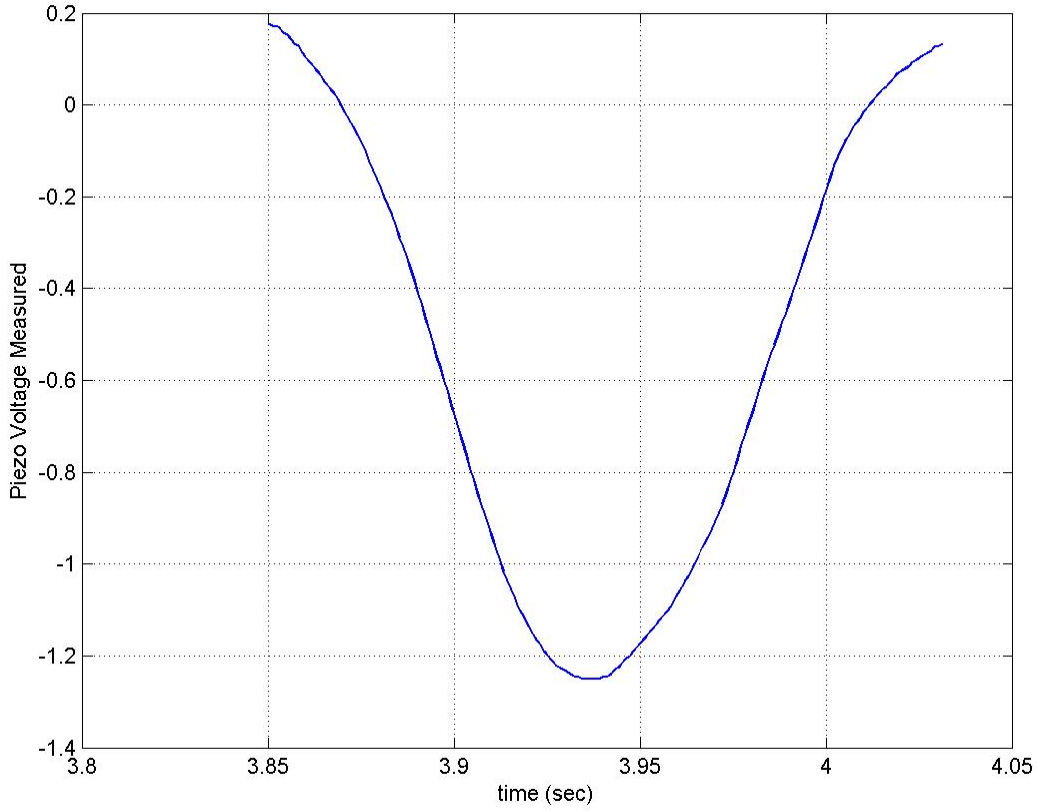

Figure 7.5 Plot showing measured piezo voltage when it was in the contact patch

Now as was discussed in chapter 4, the transfer function between measured voltage (V_L) and developed voltage (V_S) acts as a high pass filter G(s). Therefore the developed voltage is obtained by [15]:

$$V_S(s) = G^{-1}(s).V_L(s) \tag{7.1}$$

Now

$$G(s) = \frac{V_L(s)}{V_S(s)} = \frac{sR_LC_0}{1+sR_L(C_0+C_E)} \tag{7.2}$$

Hence the actual voltage developed by the piezo sensor as a result of the applied stimulus will be given by

$$V_S(s) = \left\{\frac{C_0+C_E}{C_0} + \frac{1}{sR_LC_0}\right\}V_L(s) \tag{7.3}$$

In these experiments the following values of C_0, C_E and R_L were used

a) C_0 = 2.6nF (Capacitance of the piezo film)
b) C_E = 22nF (External capacitance)
c) R_L = 22 MΩ (Load Resistance)

Figure 7.6 shows the voltage generated by the piezo film due to the applied stimulus.

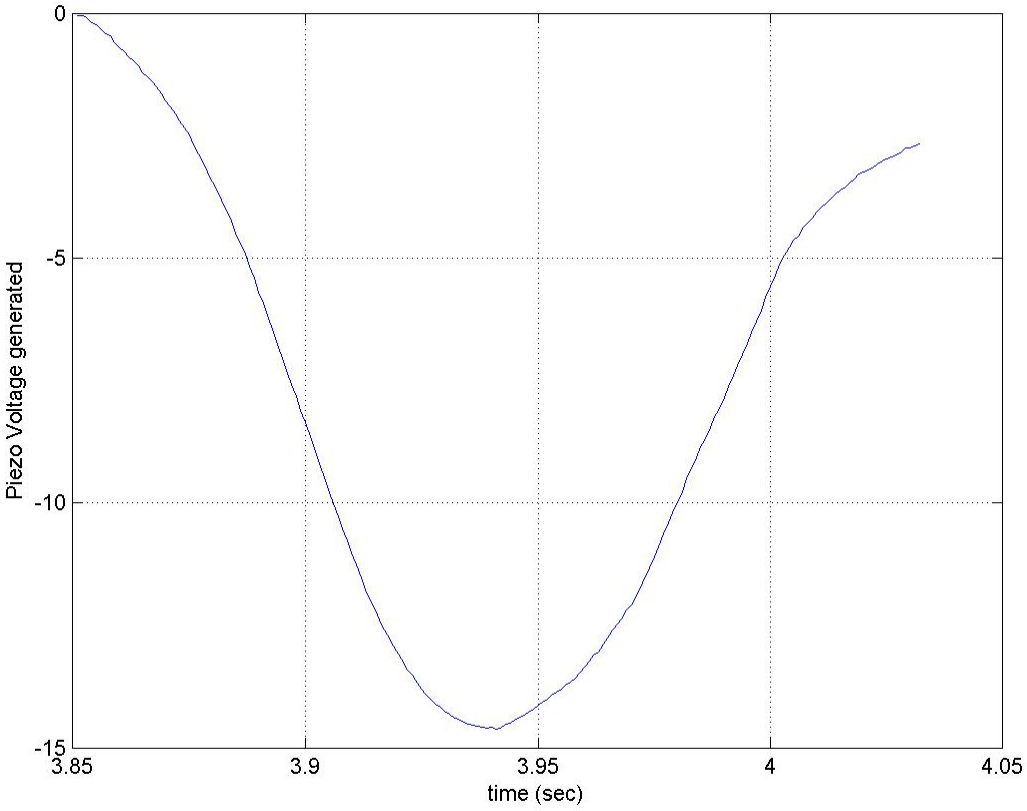

Figure 7.6 Plot showing the actual voltage generated by the piezo sensor

The above voltage signal generated by the piezo sensor is a combination of the tire deflections caused by the vertical and lateral force acting on the tire. The parameters like slip angle and friction coefficient can be estimated from the lateral deflection profile of the tire. Therefore the vertical and lateral deflections need to be separated from the above piezo signal. To do so the method of curve fitting using least mean square error has been used.

7.2 Least Mean Squares (LMS) algorithm

The least mean square method is based on the principle of minimizing the two norm of the error vector to get the optimal solution. The error vector was defined as the difference between the actual data and the function used to fit this data. The square of the error was then minimized using the 'fminsearch' function in matlab to obtain the various parameter of the desired function.

7.3 Curve Fitting

Experiments were done with different values of slip angle including zero degrees. For the zero slip case, the piezo voltage is a result of just the vertical force. The function $y = f(x)$ was used to fit the data. For the non-zero slip angle cases, the piezo voltage is a result of

vertical and lateral forces. These forces could cause a stress in the piezo in the same direction or opposite direction, as discussed in the previous chapter. Hence the function $y = f(x) \pm g(x)$ was used to fit the data, where $f(x)$ was determined in the previous step. The form of these functions and the reason for choosing them are discussed in the next section.

7.3.1 Vertical Force

The vertical force distribution along the contact patch has been assumed to be parabolic in the tire models described in Chapter 3. However the actual vertical force distribution is like a skewed parabola with the peak shifted towards the leading edge of the contact patch [16]. The resultant force also does not pass through the center of the contact patch. Figure 7.7 shows a typical normal load distribution along the contact patch.

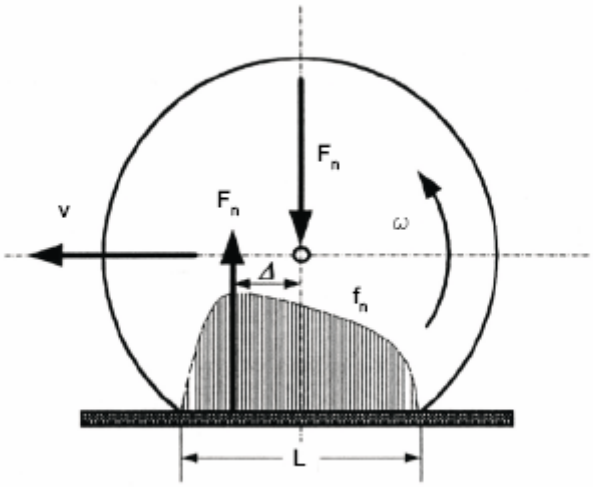

Figure 7.7 Typical normal load distribution along the contact patch [16]

The normal load distribution profile can be fitted by the following curve

$$y = f(x) \tag{5.4}$$

where $f(x)$ is chosen to be a 10^{th} order polynomial. The matlab command 'polyfit' was used to obtain the coefficients for the best fit polynomial.

7.3.2 Lateral Force

The lateral deflection profile as mentioned in the beam model follows a linear path in the static region of the contact patch, and a parabolic curve in the sliding region. Since the lateral deflection profile from the beam model consists of two functions, it cannot be directly used for curve fitting the piezo data. Therefore the following function has been proposed to approximate this deflection profile.

$$y = g(x) = \frac{(2a)\alpha}{\sin(\tan^{-1}(-\beta))} \sin\left(\tan^{-1}\left(\frac{x}{2a}\right)\right) \sin\left(\tan^{-1}\beta\left(\frac{x}{2a} - 1\right)\right) \tag{7.5}$$

where 2a is the contact patch length.

The above form of the function was inspired from the magic formula tire model which itself was obtained by fitting curves to experimental data. The parameter α in the function determines the slip angle and β determines the point at which the function will peak. For $\beta \geq 1$ the peak will occur for $a \leq x \leq 2a$. As was mentioned in the chapter on tire models that the peak of the deflection has to occur for $a \leq x \leq 2a$, therefore a value of $\beta < 1$ would imply that the tire does not have any static region. It is sliding along the entire contact patch.

The function $\frac{(2a)\alpha}{\sin(\tan^{-1}(-\beta))}\sin\left(\tan^{-1}\left(\frac{x}{2a}\right)\right)\sin\left(\tan^{-1}\beta\left(\frac{x}{2a}-1\right)\right)$ has the same approximate profile as the lateral deflection given by the beam model. Figure 7.8 shows a hypothetical lateral deflection profile as proposed by the beam model and the function used to fit this model.

The tire deflection profile is linear till $x = 7$ with a slope of $S = 2.857$ and then parabolic. The function used to fit this profile had a best fit with $\alpha = 3.4334$ and $\beta = 7.7704$.

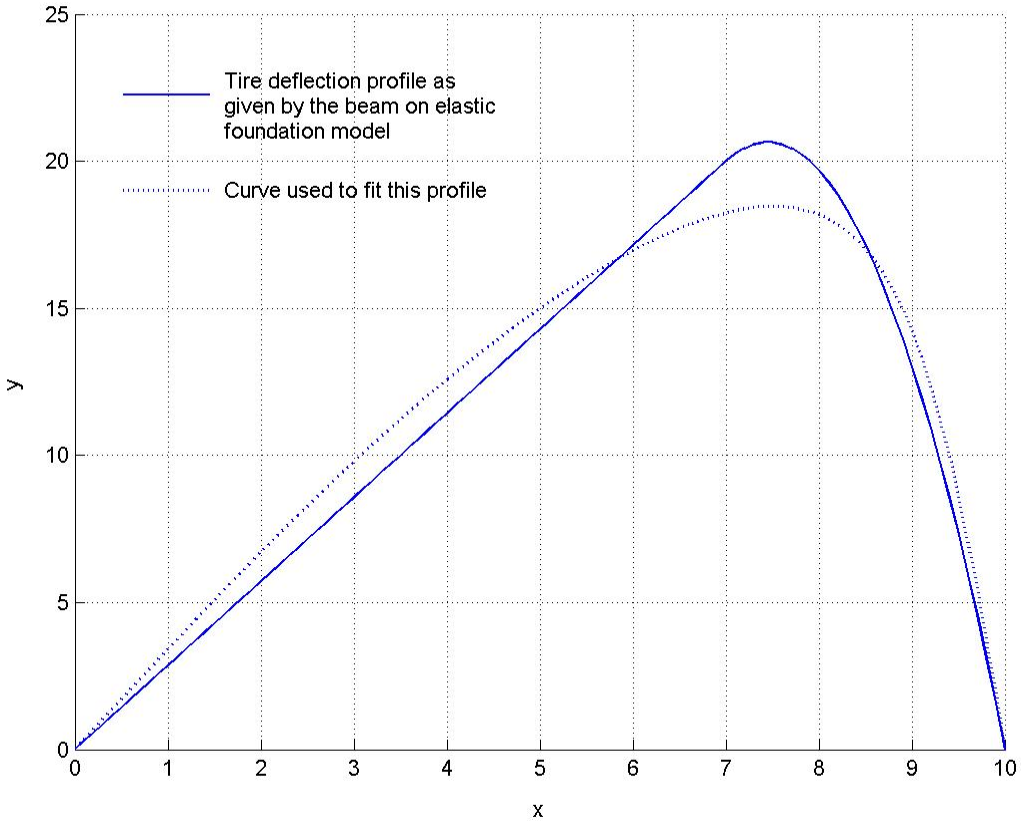

Figure 7.8 Plot showing the lateral deflection profile as proposed by the beam model and the function used to fit this profile

7.4 Significance of α and β

As mentioned earlier the value of α determines the slip angle i.e. slope of the curve in the linear region. This can be verified by differentiating the function

$$y = \frac{(2a)\alpha}{\sin(\tan^{-1}(-\beta))}\sin\left(\tan^{-1}\left(\frac{x}{2a}\right)\right)\sin\left(\tan^{-1}\beta\left(\frac{x}{2a}-1\right)\right) \tag{7.6}$$

Upon differentiation we get

$$\frac{dy}{dx} = \frac{(2a)\alpha}{\sin(\tan^{-1}(-\beta))}\left\{\frac{\cos(\tan^{-1}(x/2a))}{1+(x/2a)^2}\frac{1}{2a}\sin(\tan^{-1}\beta(\frac{x}{2a}-1))\right.$$
$$\left. + \frac{\cos(\tan^{-1}\beta(x/2a-1))}{1+\beta^2(x/2a-1)^2}\frac{\beta}{2a}\sin(\tan^{-1}(\frac{x}{2a}))\right\} \tag{7.7}$$

At $x = 0$ the slope is

$$\left.\frac{dy}{dx}\right|_{x=0} = \frac{(2a)\alpha}{\sin(\tan^{-1}(-\beta))}\left[\frac{\sin(\tan^{-1}(-\beta))}{2a}+0\right] \tag{7.8}$$
$$= \alpha \tag{7.9}$$

The slope at $x = 0$ is independent of β and $2a$. Therefore the value of α gives the slope of the linear part of the deflection profile.

It was also mentioned that the value of β determines the point at which the function will peak. To verify this we must set the derivative of the function equal to zero. Equation 7.7 can be rewritten as

$$\frac{dy}{dx} = \frac{(2a)\alpha}{\sin(\tan^{-1}(-\beta))}\left\{\frac{1/2a}{(1+(x/2a)^2)^{3/2}}\frac{\beta(x/2a-1)}{\sqrt{1+\beta^2(x/2a-1)^2}}+\frac{\beta/2a}{(1+\beta^2(x/2a-1)^2)^{3/2}}\frac{x/2a}{\sqrt{1+(x/2a)^2}}\right\} \tag{7.10}$$

$$\frac{dy}{dx} = 0$$

$$\Rightarrow \frac{\beta}{2a}\left(\frac{x}{2a}-1\right)\left(1+\beta^2\left(\frac{x}{2a}-1\right)^2\right)+\frac{\beta}{2a}\frac{x}{2a}\left(1+\left(\frac{x}{2a}\right)^2\right)=0 \tag{7.11}$$

Setting $y = x/2a$ we get

$$\begin{aligned}&(y-1)\left(1+\beta^2(y-1)^2\right)+y\left(1+y^2\right)=0\\ &\Rightarrow(\beta^2+1)y^3+(-3\beta^2)y^2+(3\beta^2+2)y+(-\beta^2-1)=0\end{aligned} \tag{7.12}$$

Therefore if the value of β is known then the above equation can be solved for x to obtain the point at which the function peaks i.e. $x_{\max}$. Using the value of $x_{\max}$ the value of x_s can be calculated as follows (Refer to equation 5.22)

$$x_s = \sqrt{2(2a)x_{\max}-(2a)^2} \tag{7.13}$$

In the above example (refer to figure 7.8) the value of α obtained was 3.4334 and the actual value of slope was 2.857. Also β was 7.7704. Solving the cubic equation we get $x_{\max} = 7.514$. Substituting $x_{\max} = 7.514$ and $2a = 10$ in the above equation we get $x_s = 7.0908$ which is close to the actual value of x_s which is 7.

Chapter 8

RESULTS

Table 8.1 lists the different conditions under which the experiments were conducted. The speed of the scooter was constant in all these experiments and equal to 0.375m/s. Weight of 100lbs corresponded to a vertical force of 173.25N on the tire and the weight of 80lbs corresponded to a vertical force of 138.6N (Equation 6.1).

Surface	Weight used (lbs)	Slip angle (degrees)
Rough (Carpet)	100	0, 4, 8,12
Smooth (Floor)	100	0, 4, 8,12
Smooth (Floor)	80	0, 4, 8,12

Table 8.1 Table showing the different experimental setups

8.1 Experimental Results for a carpet

The following experiment was done on a carpet (high friction coefficient surface). The tire was set at a slip angle of 0, 4, 8 and 12 degrees and the piezo output voltage was measured in each case. In this experimental setup the vertical and lateral forces produced stresses in opposite directions, hence the piezo voltage showed a decrease with increase in slip angle. Figure 8.1 shows the piezo voltage for different values of slip angle. Note that the contact patch length in this case is about 0.09m.

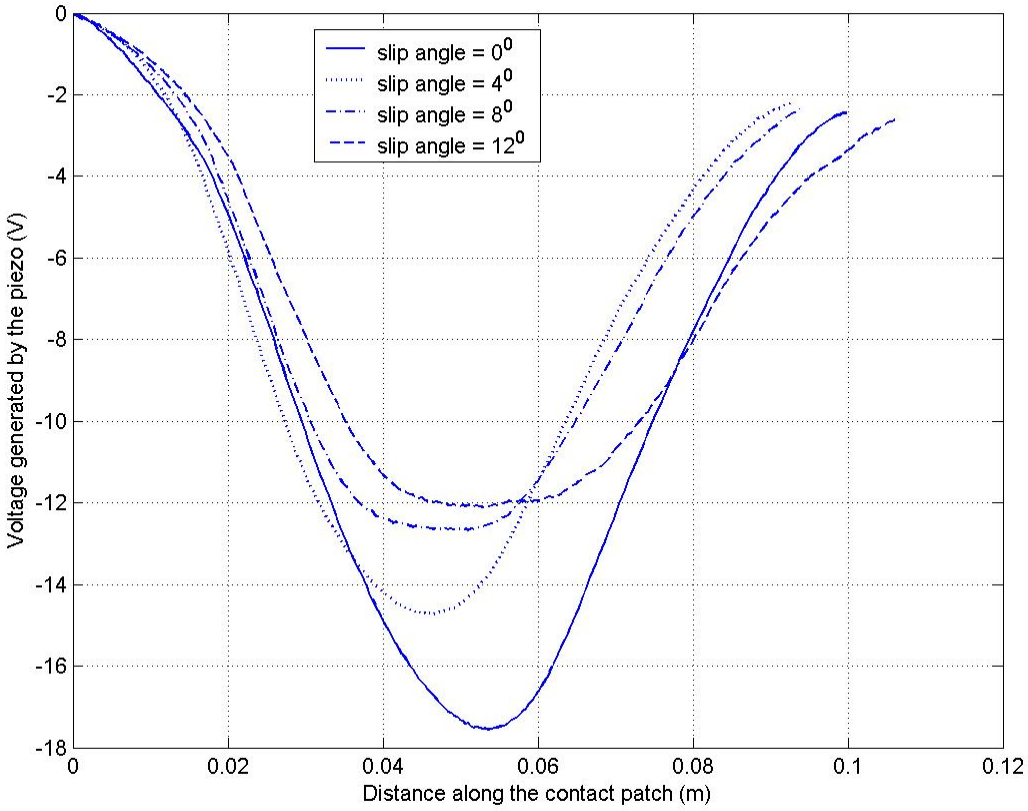

Figure 8.1 Piezo Voltage for different values of slip angle

Figure 8.2 shows the zero slip angle data and the corresponding 10th order polynomial used to fit this data.

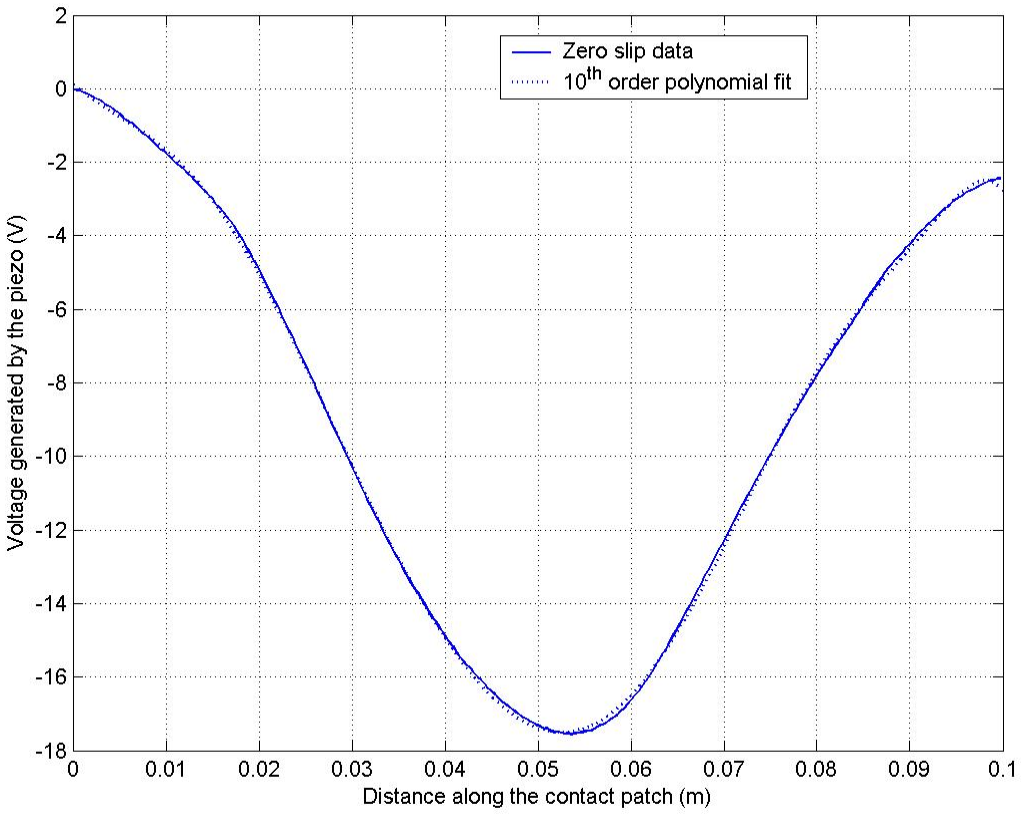

Figure 8.2 Plot of zero slip data and the 10th order polynomial used to fit this data

The 10th order polynomial which best fit this data has the following form

$$y = p_1x^{10} + p_2x^9 + p_3x^8 + p_4x^7 + p_5x^6 + p_6x^5 + p_7x^4 + p_8x^3 + p_9x^2 + p_{10}x + p_{11}$$

with

p_1 = -3.6919e+014

p_2 = 1.6858e+014

p_3 = -3.2249e+013

p_4 = 3.3523e+012

p_5 = -2.0423e+011

p_6 = 7.1725e+009

p_7 = -1.2259e+008

p_8 = 3.1672e+005

p_9 = 6739.3

p_{10} = -210.93

p_{11} = 0.14407

Figure 8.3 shows the plot of slip angle = 4^0. The polynomial obtained above and the proposed function was used to fit this plot.

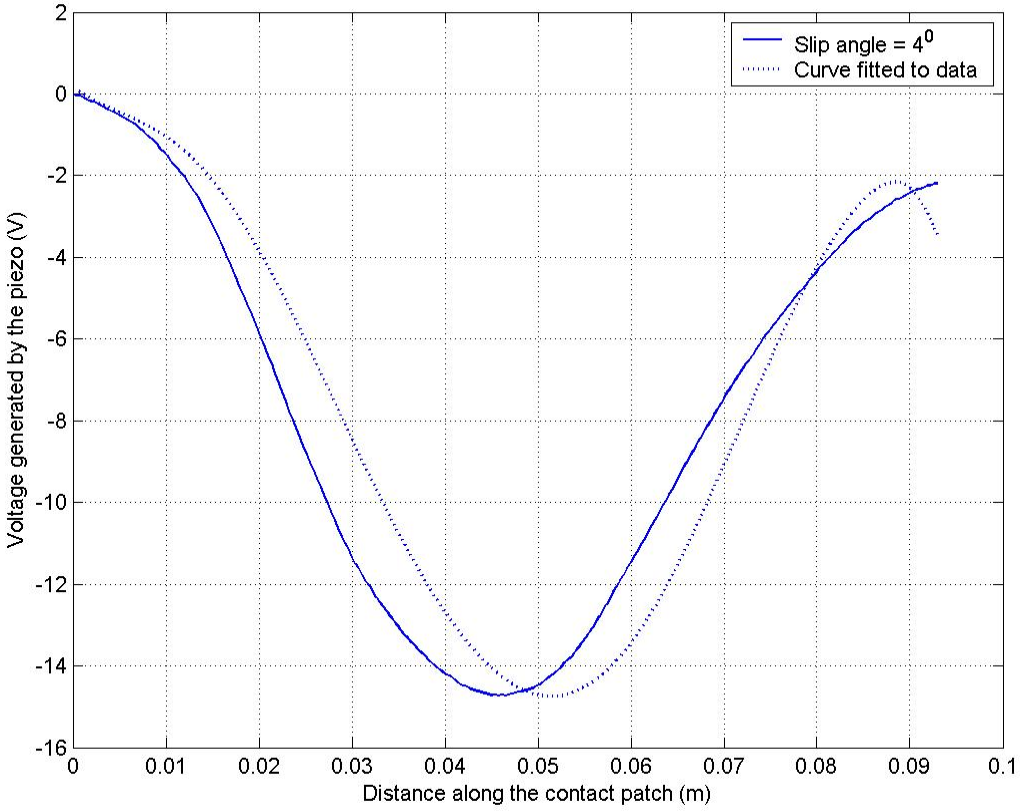

Figure 8.3 Plot showing piezo signal obtained for slip angle = 4^0 and the curve fitted to this data

The value of α and β obtained were -60.4243 and 11.3456 respectively. Using β gives $x_{\max}$ = 0.0740, which gives x_s = 0.0715.

The value of α from this experiment was used as a reference to calculate the linear interpolation constants between the slope of the piezo voltage (α) and slip angle. The relation slip angle $= -a\alpha - b$ with $a = 0.14$ and $b = 4$ were determined. These constants will also be used in results obtained from other experiments.

For the carpet it has been assumed that $\mu = 1$. Using the relation $x_s = 2a(1-\theta S)$ with $\theta = \dfrac{4a^2 bk}{3\mu F_z}$, S = tan(4), 2a = 0.09m and $F_z = 173.25\,\text{N}$ we get bk = 38234.26. This constant will be used in the results obtained from the other experiments.

Figure 8.4 shows the plot for slip angle = 8^0 and the curve fitted to this data.

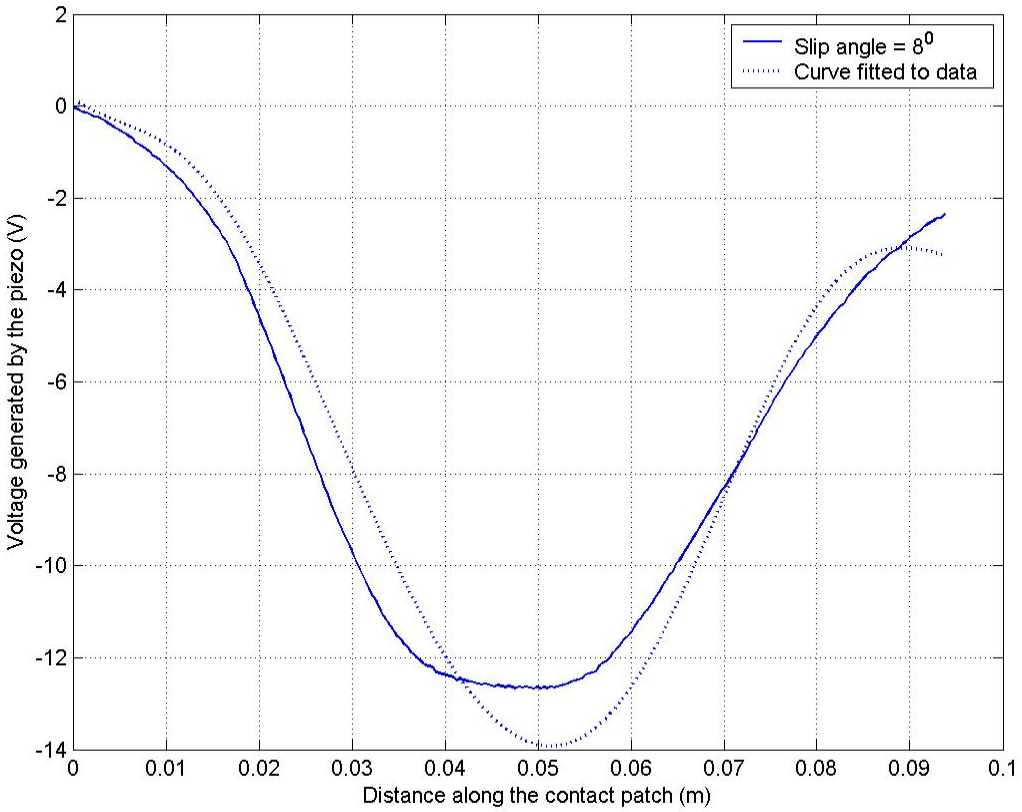

Figure 8.4 Plot showing piezo signal obtained for slip angle = 8^0 and the curve fitted to this data

The value of α and β obtained were -84.3996 and 4.5873 respectively. Using β gives x_{max} = 0.0639, which gives x_s = 0.0565. The value of α =-84.3996 would corresponds to a slip angle of 7.76^0.

Figure 8.5 shows the plot for slip angle = 12^0 and the curve fitted to this data.

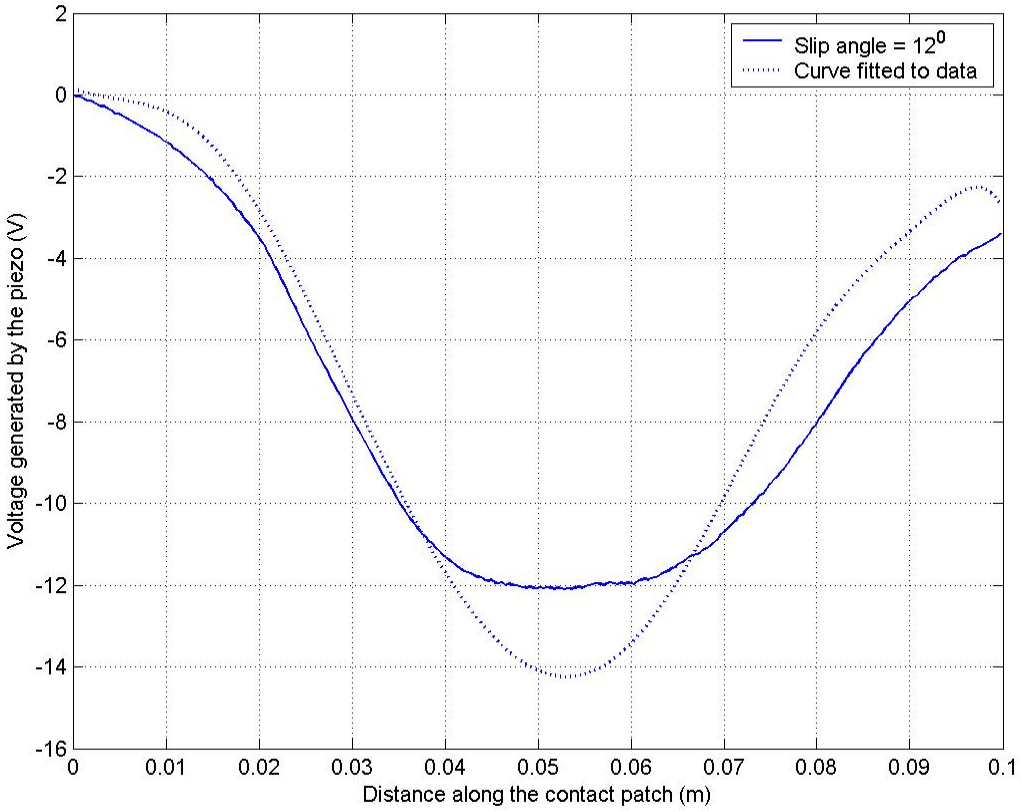

Figure 8.5 Plot showing piezo signal obtained for slip angle = 12^0 and the curve fitted to this data

The value of α and β obtained were -119.37 and 2.9731e-6 respectively. Since $\beta < 1$, the tire does not have a static region and is sliding along the entire contact patch. The value of the tire-road friction coefficient cannot be predicted in this case. The value of $\alpha = -119.37$ using the same linear relations as before yields a slip angle value of 12.8^0.

8.2 Experimental results for a smooth surface and 100lbs of load

The following experiment was done on the floor (smooth surface). The tire was set at a slip angle of 0, 4, 8 and 12 degrees and the piezo output voltage was measured in each case. In this experimental setup the vertical and lateral forces produced stresses in opposite directions, hence the piezo voltage showed a decrease with increase in slip angle. Figure 8.6 shows the piezo voltage for different values of slip angle.

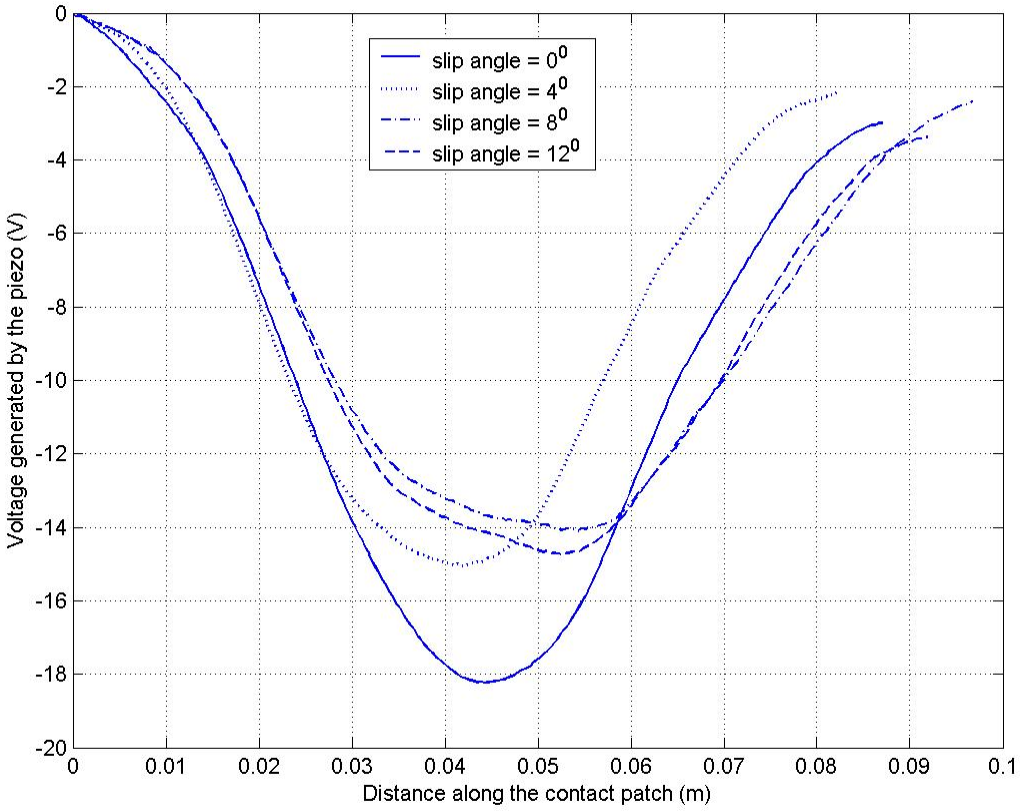

Figure 8.6 Piezo Voltage for different values of slip angle

Figure 8.7 shows the zero slip angle data and the corresponding 10th order polynomial used to fit this data.

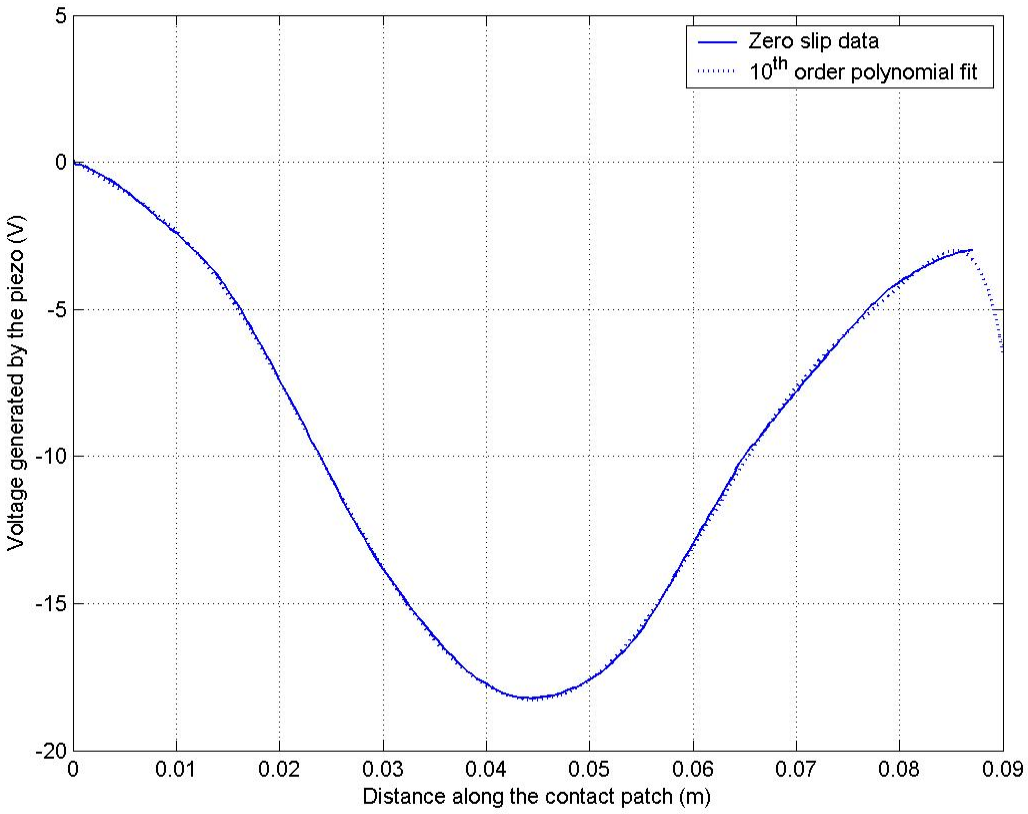

Figure 8.7 Plot of zero slip data and the 10th order polynomial used to fit this data

The 5th order polynomial which best fit this data has the following form

$$y = p_1x^{10} + p_2x^9 + p_3x^8 + p_4x^7 + p_5x^6 + p_6x^5 + p_7x^4 + p_8x^3 + p_9x^2 + p_{10}x + p_{11}$$

with

p_1 = -1.6648e+015
p_2 = 6.6928e+014
p_3 = -1.1296e+014
p_4 = 1.0382e+013
p_5 = -5.607e+011
p_6 = 1.7575e+010
p_7 = -2.79e+008
p_8 = 1.2848e+006
p_9 = 1016.8
p_{10} = -230.88
p_{11} = 0.08749

Figure 8.8 shows the plot for slip angle = 4^0. The polynomial obtained above and the proposed function was used to fit this plot.

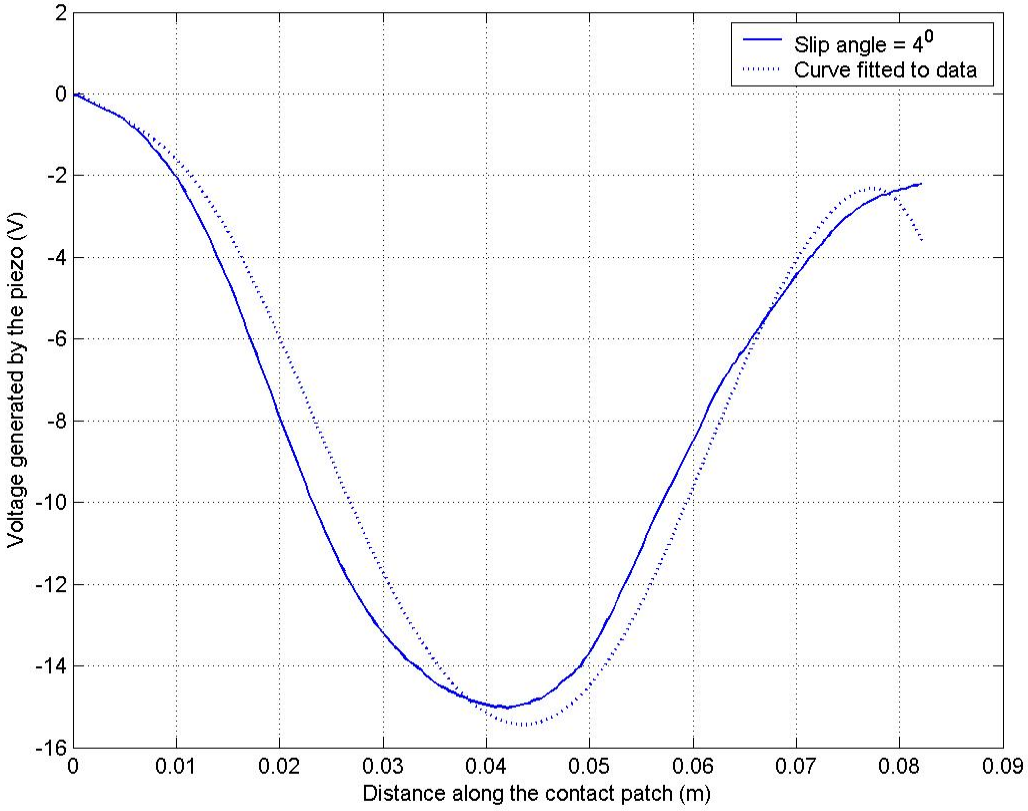

Figure 8.8 Plot showing piezo signal obtained for slip angle = 4^0 and the curve fitted to this data

The value of α and β obtained were -73.0574 and 14.7835 respectively. Using β gives x_{max} = 0.0676, which gives x_s = 0.0660.

Figure 8.9 shows the plot for slip angle = 8^0 and the curve fitted to this data.

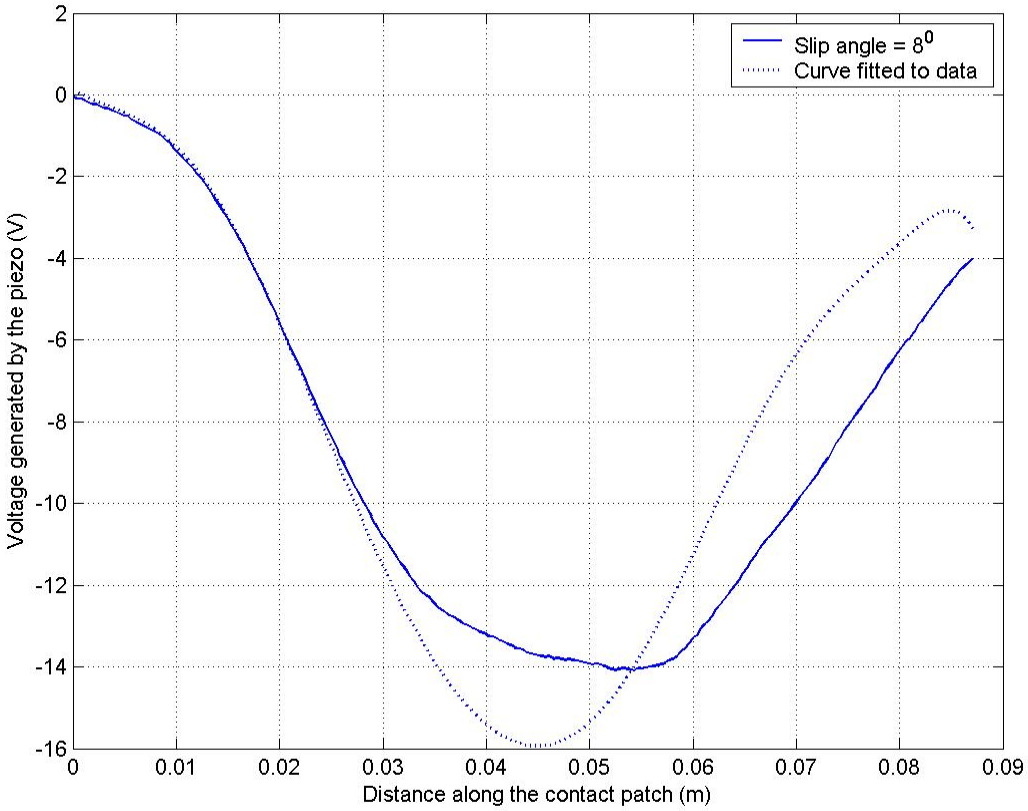

Figure 8.9 Plot showing piezo signal obtained for slip angle = 8^0 and the curve fitted to this data

The value of α and β obtained were -119.9513 and 8.1888e-007 respectively. Since $\beta < 1$, the tire does not have a static region and is sliding along the entire contact patch. The value of α cannot be predicted in this case.

Figure 8.10 show the plot for slip angle = 12^0 and the curve fitted to this data.

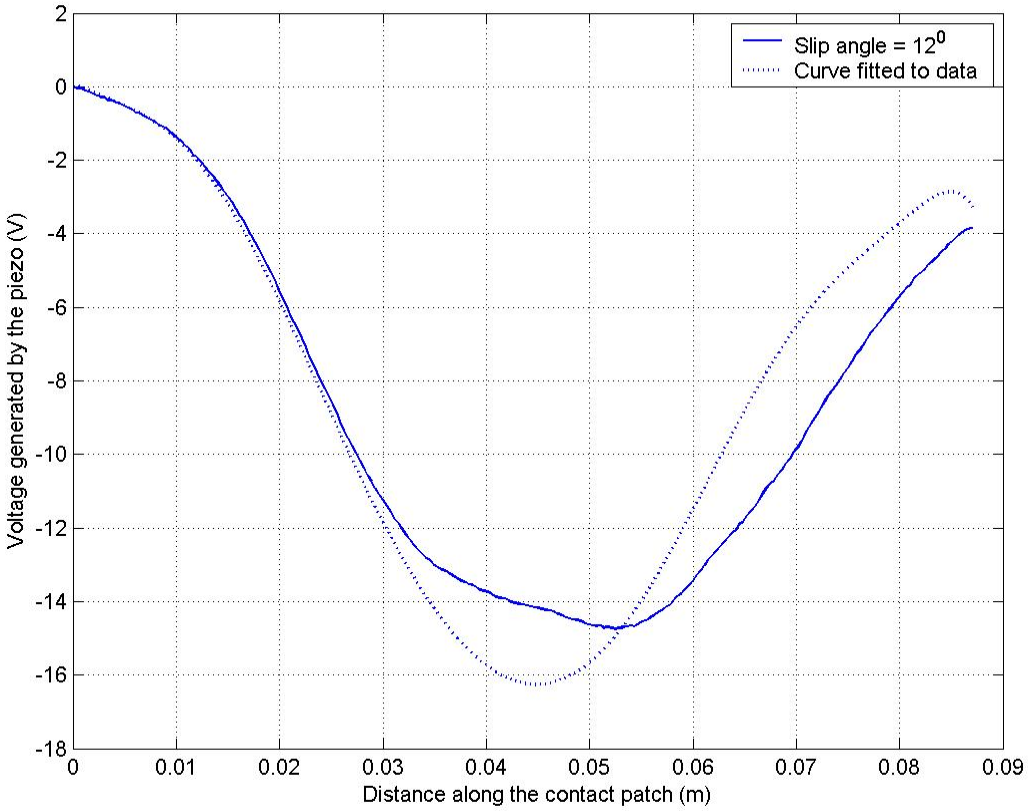

Figure 8.10 Plot showing piezo signal obtained for slip angle = 12^0 and the curve fitted to this data

The value of α and β obtained were - 103.4426 and 2.7639e-007 respectively. Since $\beta < 1$, the tire does not have a static region and is sliding along the entire contact patch. The value of α cannot be predicted in this case.

8.3 Experimental results for a smooth surface and 80lbs of load

The following experiment was done on the floor (smooth surface). The tire was set at a slip angle of 0, 4, 8 and 12 degrees and the piezo output voltage was measured in each case. In this experimental setup the vertical and lateral forces produced stresses in the same direction, hence the piezo voltage showed an increase with increase in slip angle. Figure 8.11 shows the piezo voltage for different values of slip angle. The contact patch length in this case is about 0.85m.

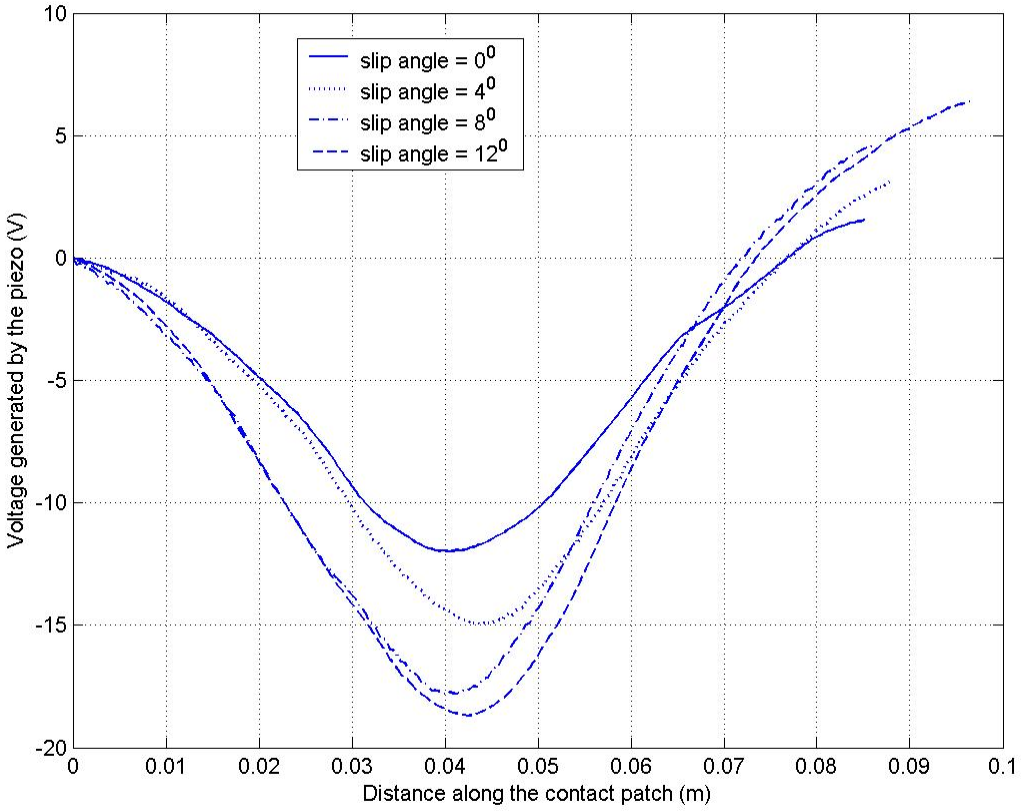

Figure 8.11 Piezo Voltage for different values of slip angle

Figure 8.12 shows the zero slip angle data and the corresponding 10th order polynomial used to fit this data.

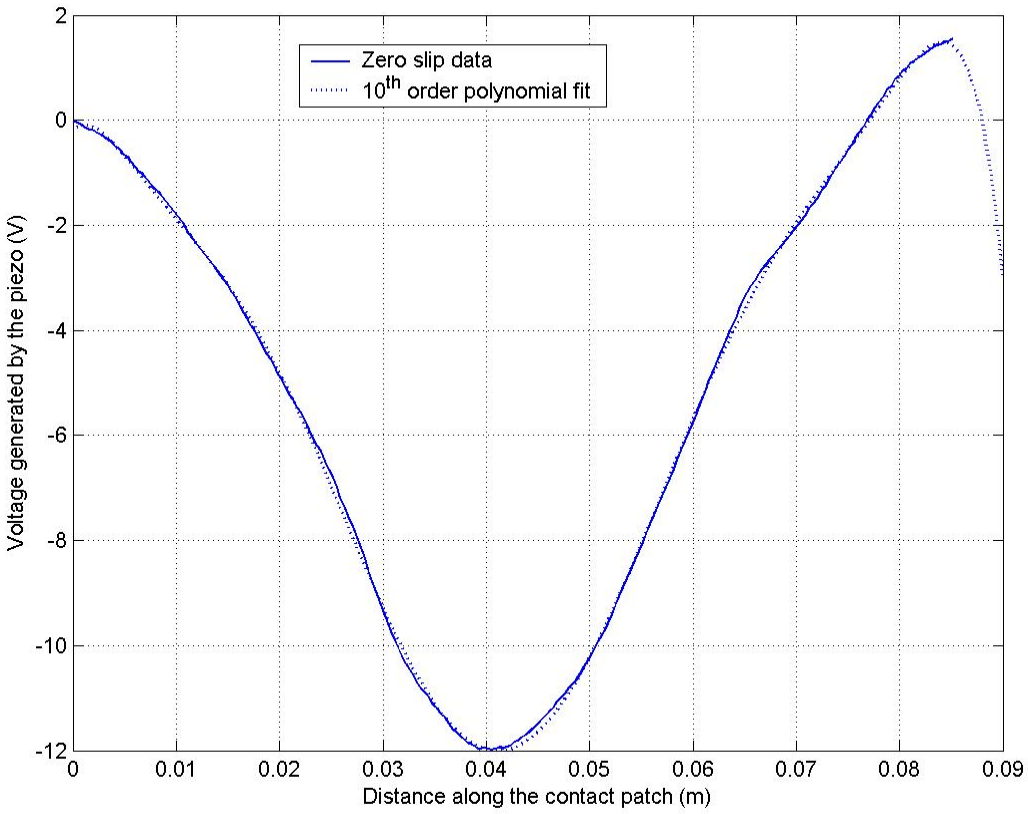

Figure 8.12 Plot of zero slip data and the 10th order polynomial used to fit this data

The 10th order polynomial which best fit this data has the following form

$$y = p_1x^{10} + p_2x^9 + p_3x^8 + p_4x^7 + p_5x^6 + p_6x^5 + p_7x^4 + p_8x^3 + p_9x^2 + p_{10}x + p_{11}$$

with

p_1 = -7.02e+014

p_2 = 3.1403e+014

p_3 = -6.3092e+013

p_4 = 7.4144e+012

p_5 = -5.4922e+011

p_6 = 2.5641e+010

p_7 = -7.2108e+008

p_8 = 1.1433e+007

p_9 = -98183

p_{10} = 181.83

p_{11} = -0.17526

Figure 8.13 shows the plot for slip angle = 4^0. The polynomial obtained above and the proposed function was used to fit this plot.

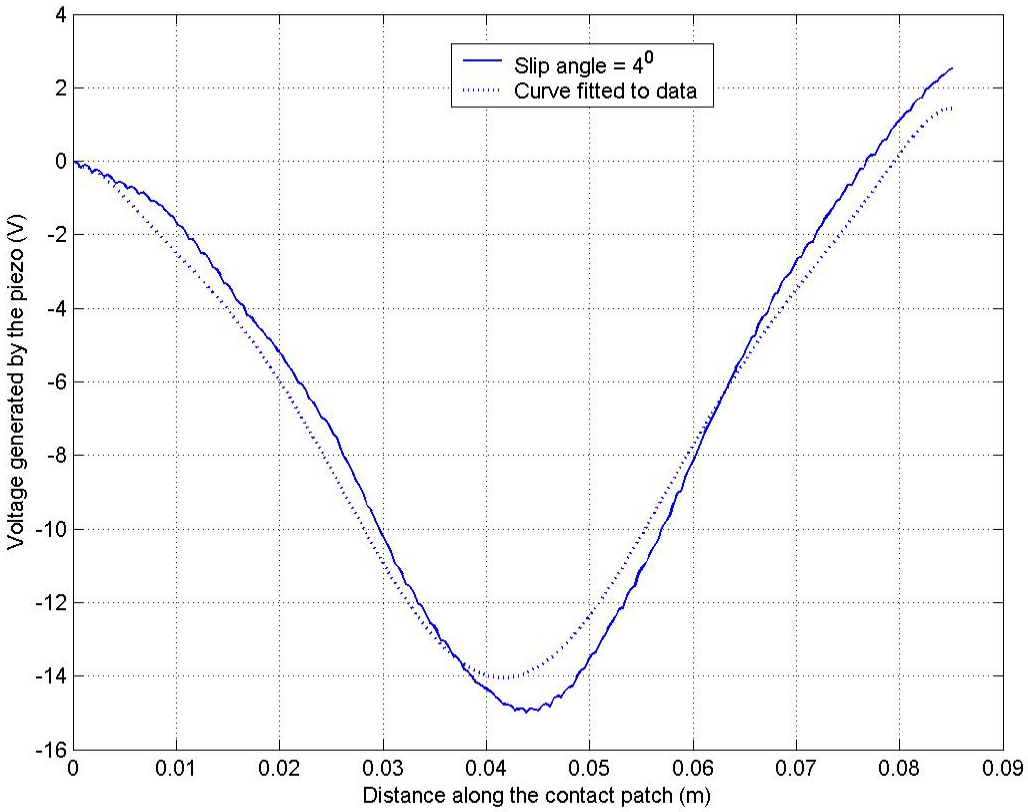

Figure 8.13 Plot showing piezo signal obtained for slip angle = 4^0 and the curve fitted to this data

The value of α and β obtained were 64.4914 and 2.8446 respectively. Using β gives $x_{\max}$ = 0.0523, which gives x_s = 0.0407.

Figure 8.14 shows the plot for slip angle = 8^0 and the curve fitted to this data.

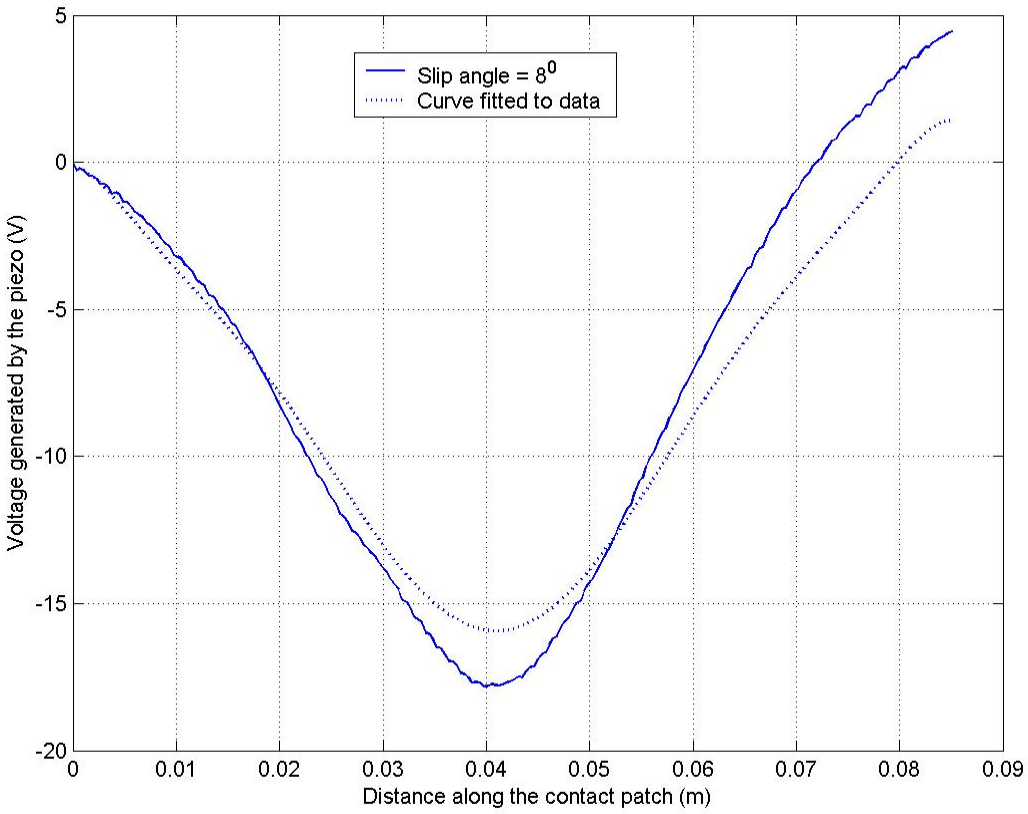

Figure 8.14 Plot showing piezo signal obtained for slip angle = 8^0 and the curve fitted to this data

The value of α and β obtained were 208.2912 and 2.5943e-7 respectively. Since $\beta < 1$, it means that the tire does not have any linear region and is sliding along the entire contact patch. The value of α cannot be predicted in this case.

Figure 8.15 shows the plot for slip angle = 12^0 and the curve fitted to this data.

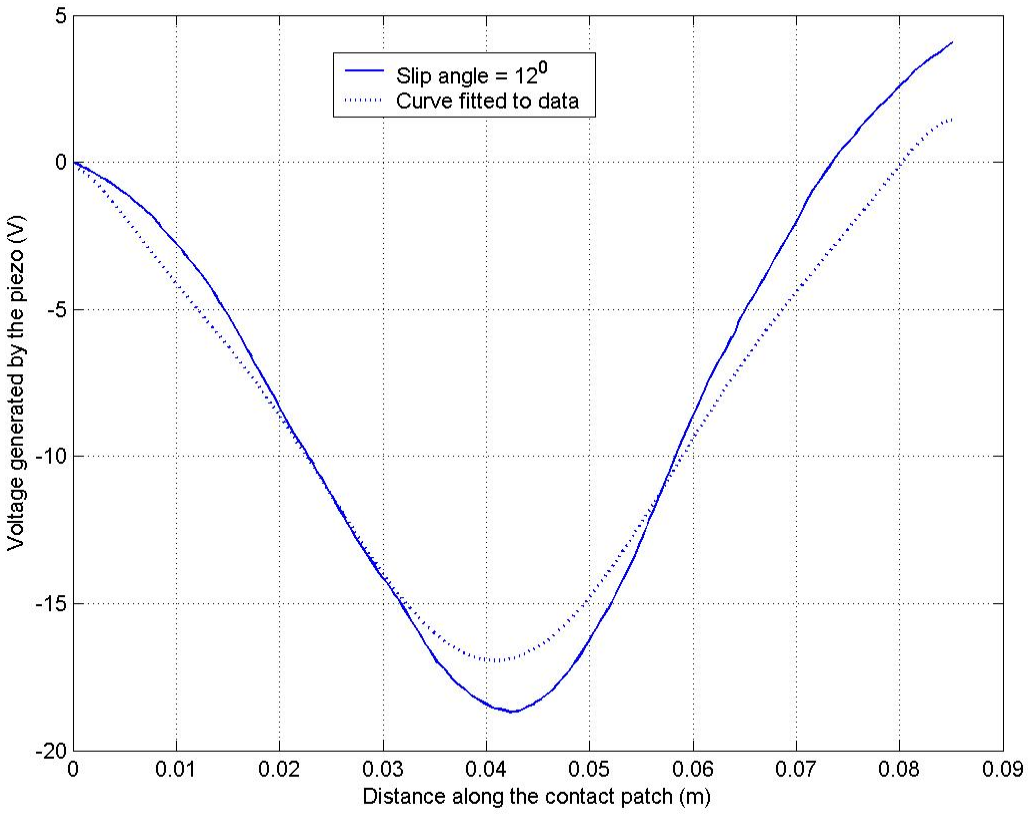

Figure 8.15 Plot showing piezo signal obtained for slip angle = 12^0 and the curve fitted to this data

The value of α and β obtained were 257.5546 and 0.1967 respectively. Since $\beta < 1$, it means that the tire does not have any linear region and is sliding along the entire contact patch. The value of α cannot be predicted in this case.

8.4 Summary of results

Table 8.2 presents a summary of the estimated values of slip angle and friction coefficient obtained from the results shown above.

Table 8.2 Table showing the summary of results obtained

Experimental conditions	**Slip angle**		**Estimated μ using estimated slip angle**	**Estimated μ using actual slip angle**
	Actual	**Estimate**		
Carpet Weight = 100lbs	4 8 12	4.4 7.76 12.8	1 0.873 -	1 0.9 -
Floor Weight = 100lbs	4 8 12	4.83 - -	0.755 - -	0.625 - -
Floor Weight = 80lbs	4 8 12	4.27 - -	0.427 - -	0.38 - -

Chapter 9

CONCLUSIONS

Real-time measurement of tire-road friction coefficient is extremely valuable for winter road maintenance operations. Knowledge of tire-road friction coefficient can be used to optimize the kind and quantity of the deicing and anti-icing chemicals applied to the roadway.

In this project, a wheel based tire-road friction coefficient measurement system was first developed for snowplows. Unlike a traditional Norse meter, this system is based on measurement of lateral tire forces, has no moving parts and does not use any actuators. Hence, it is reliable and inexpensive. A key challenge is quickly detecting changes in estimated tire-road friction coefficient while rejecting the high levels of noise in measured force signals. Novel filtering and signal processing algorithms are developed to address this challenge including a biased quadratic mean filter and an accelerometer based vibration removal filter.

Detailed experimental results were presented on the performance of the friction estimation system on different types of road surfaces. Experimental results show that the biased quadratic mean filter works very effectively to eliminate the influence of noise and quickly estimate changes in friction coefficient. Further, the use of accelerometers and an intelligent algorithm enables elimination of the influence of driver steering maneuvers, thus providing a robust friction measurement system.

In the second part of the project, the developed friction measurement system is used for automated control of the chemical applicator on the snowplow. An electronic interface is established with the Force America applicator to enable real-time control. A feedback control system that utilizes the developed friction measurement sensor and a pavement temperature sensor is developed and implemented on the snowplow. The working of the automated control system is documented through videos.

Finally, an unsuccessful initial research explored in the project was to use piezeoelectric sensors to measure tire deflections. Tire deflections could be related to the friction coefficient. This approach also provided a means to simultaneously measure slip angle without having to use any additional sensors. Piezo sensors were chosen for this task as they directly provided voltage as the output without a need for any external power supply. Also they had a longer life and were cheaper compared to other conventional sensors. Some of the specific conclusions of this part of the work are outlined below.

(i) The piezo sensors are sensitive but are not smart sensors. Or in other words they are significantly affected by the environment they are being used in. This was evident in the piezo output obtained when different configurations were tried out for the tire. Also since the piezo sensor was pasted to the tire, in situations when it would come off and would be pasted

back again, the output given by the sensor was not identical as before. This was because slight misalignment from the previous setting would affect the sensor.

(ii) The simplified form to the beam on elastic foundation model provides a good approximation for the actual tire deflection profile. It also provides a relationship between $x_{\max}$ and x_s which simplifies estimation of the variable x_s. This is not possible if the elastic foundation model is used as in that model there is no relation between $x_{\max}$ and x_s if x_s lies between 0 and 'a' i.e. in the first half of the contact patch. The function proposed in section 5.3.2 to fit the lateral deflection profile of the tire also provides a good fit for the tire deflection profile as given by the beam model, which is a combination of two different curves.

(iii) The results obtained are consistent with the proposed theory of tire models. The piezo voltage showed a change (increase or decrease depending on direction of lateral force) for values of slip angle other than zero. The voltage output starts to saturate for higher values of slip angle (8^0 and 12^0). This is because as the tire starts slipping along the entire contact patch (i.e. $x_s = 0$), any further increase in slip angle won't affect the tire deflection.

(iv) Experimental results for estimation of tire road friction coefficient could only be obtained reliably in a few cases due to excessive slip along the tire contact patch in many of the experiments. A better experimental set-up in which significantly higher normal loads can be applied to the tires might help address this issue. Based on the experiments conducted thus far, tire-road friction coefficient could not be reliably estimated.

REFERENCES

[1] Y. Fukada, "Slip-Angle Estimation for Vehicle Stability Control", *Vehicle System Dynamics*, 32 (1999), pp. 375-388.

[2] J. H. Park, and C. Y. Kim, "Wheel Slip Control in Traction Control System for Vehicle Stability", *Vehicle System Dynamics*, 31 (1999), pp. 263-278.

[3] R. Rajamani, "Lateral Vehicle Dynamics", *Vehicle Dynamics and Control*, Springer Verlag, ISBN 978-0-387-2639-0, 2005.

[4] Jin-Oh Hahn, R. Rajamani, and L. Alexander, "GPS-Based Real-Time Identification of Tire-Road Friction Coefficient", *IEEE Transactions on Control Systems Technology*, Vol. 10, No. 3, May 2002.

[5] J. Wang, P. Agrawal, L. Alexander, and R. Rajamani, "An Experimental Study with Alternate Measurement Systems for Estimation of Tire-Road Friction Coefficient", *American Control Conference*, Proceedings of the 2003, Vol. 6, June 2003, pp. 4957-4962.

[6] Piezo Film Sensors, *Technical Manual*, Measurement Specialties Inc., www.msiusa.com

[7] J. Y. Wong, "Mechanics of Pneumatic Tires", *Theory of Ground Vehicles*, 3rd Edition, Chapter 1, ISBN 0-471-35461-9.

[8] R. Rajamani, "Generation of Lateral Tire Forces", copyright © 2001.

[9] C. S. Liu, and H. Peng, "Road Friction Coefficient Estimation for Vehicle Path Prediction", *Vehicle System Dynamics*, Vol. 25 Suppl., 1996, pp. 413-425.

[10] J. P. Maurice, M. Berzeri, and H. B. Pacejka, "Pragmatic Tyre Model for Short Wavelength Side Slip Variations", *Vehicle Systems Dynamics*, Vol. 31 (1999), pp. 65-94.

[11] J. Lacombe, "Tire Model for Simulations of Vehicle Motion on High and Low Friction Road Surfaces", *Simulation Conference Proceedings*, Winter (2000), Vol. 1, pp. 1025-1034.

[12] H. B. Pacejka, “The Tyre as a Vehicle Component”, XXVI Fisita Congress Prague, June 16-23, 1996.

[13] J. C. Dixon, “The tyre”, *Tyres, Suspension and Handling*, 1st Edition, Chapter 2, ISBN 0-521-40194-1.

[14] M. Gäfvert, “Topics in Modeling, Control and Implementation in Automotive Systems”, *PhD thesis*, Department of Automatic Control, Lund Institute of Technology, Sweden.

[15] S. W. Kim, I. Cho, J. H. Lee, J. Park, D. H. Yi and D. Cho, “A New Method for Accurately Estimating the Weight of Moving Vehicles Using Piezoelectric Sensors and Adaptive-footprint Tire Model”, *Vehicle System Dynamics*, 2003, Vol. 39, No. 2, pp. 135-148.

[16] C. Canudas-de-Wit, P. Tsiotras, E. Velenis, M. Basset, G. Gissinger, “Dynamic Friction Models for Road/Tire Longitudinal Interactions”, *Vehicle System Dynamics*, 2003, Vol. 39, No. 3, pp. 189-226.

[17] R. Späth, “Instrumented Wheel for the Measurement of Rear Axle Wheel Force”, *Agrartechnische Forschung* 7 (2001) Heft 5, S. E 86 – E 91.

[18] H. Itoh, A. Oida, and M. Yamazaki, “Measurement of Forces Acting on 4WD-4WS Tractor Tires during Steady State Circular Turning in a Rice Field”, *Journal of Terramechanics*, Vol. 32, No. 5, pp. 263-283, 1995.

[19] A. Pohl, R. Steindl, L. Reindl, “The Intelligent Tire Utilizing Passive SAW Sensors – Measurement of Tire Friction”, *IEEE Transactions on Instrumentation and Measurement*, Vol. 48, No. 6, December 1999.

[20] I. L. Al-Qadi, A. Loulizi, G. W. Flintsch, D. S. Roosevelt, R. Decker, J. C. Wambold, W. A. Nixon, “Feasibility of Using Friction Indicators to Improve Winter Maintenance Operations and Mobility”, *NCHRP Web Document* 53, November 2002.

[21] J. Wang, P. Agrawal, L. Alexander, R. Rajamani, “An Experimental Study with

Alternate Measurement Systems for Estimation of Tire-Road Friction Coefficient", Proceedings of the 2003 *American Control Conference*, Denver, Colorado, June 2003.

[22] R. Rajamani, *Vehicle Dynamics and Control*, Springer Verlag, ISBN: 978-0-387-26396-0, 2005.

[23] I. Miller, J.E. Freund, *Probability and Statistics for Engineers*, ISBN: 978-0-131-43745-6, Aug 2004.

[24] F. Gustafsson, "Estimation and Change Detection of Tire – Road Friction Using the Wheel Slip", Proceedings of the 1996 *IEEE International Symposium on Computer-Aided Control System Design*, Dearborn, MI September 15-18,1996.

[25] F. Gustafsson, "Slip-based tire-road friction estimation," *Automatica*, vol. 33, no. 6, pp. 1087–1099, June 1997.

[26] James Lacombe, "Tire Model for Simulations of Vehicle Motion on High and Low Friction Road Surfaces", Proceedings of the 2000 *Winter Simulation Conference*, 2000.

[27] J. O. Hahn, R. Rajamani, A. Lee, "GPS-based real-time identification of tire-road friction coefficient", *IEEE Transactions on Control Systems Tech*., v 10, n 3, May, 2002, p 331-343.

[28] S. Muller, M. Uchanski, K. Hedrick, "Estimation of the Maximum Tire-Road Friction Coefficient", *Journal of Dynamic Systems, Measurement and Control*, Transactions of the ASME, v 125, n 4, December, 2003, p 607-617.